Aalto University
School of Electrical Engineering
Bioinformation Technology
Master's Thesis

Brain mechanisms of sensory and vicarious pain

Tomi Karjalainen

12.12.2014

Instructor and supervisor:

Prof. Lauri Nummenmaa

AALTO UNIVERSITY
SCHOOL OF ELECTRICAL ENGINEERING

ABSTRACT OF
THE MASTER'S THESIS

Author Tomi Karjalainen

Title Brain mechanisms of sensory and vicarious pain

Degree programme Bioinformation technology

Thesis supervisor Prof. Lauri Nummenmaa

Department of Biomedical Engineering and Computational Science

Thesis instructor Prof. Lauri Nummenmaa

Date 12.12.2014 **Number of pages** 40 **Language** English

Abstract

The aim of the Thesis was to study the brain circuits representing sensory and vicarious pain. Experiments with functional magnetic resonance imaging were conducted to study neural activity patterns evoked by both stimulus modalities. Sensory pain was induced to subjects by applying noxious heat to right foot, while pictures of painful feet were used to arouse vicarious pain. Sensory pain was modeled in three different ways within the framework of the general linear model: The event-like model assumes that brain's pain-circuits are activated only during noxious stimulus, while the two other models that used long and intermediate blocks additionally assume, to different degrees, that also expectation of pain activates the same circuits.

Both sensory and vicarious pain triggered robust neural activity increase in partly overlapping but mostly neighboring clusters in an area extending bilaterally from midcingulate cortex to supplementary motor area. The self-related pain cluster located slightly posterior to the other-related cluster. Stimulus-modality-specific brain regions exhibiting increased activation included somatosensory cortex and bilateral anterior insula for sensory pain and occipital cortex for vicarious pain. Among the tested models of pain perception, the event-like model yielded results that most closely match previously reported findings.

Overall, the results of the Thesis accord with prior literature, and thus confirm the suitability of the selected stimuli and experimental design for studying brain circuits representing pain. Help-promotion is suggested to account for the partly shared neural representations of sensory and vicarious pain. The results and the model's straightforward interpretability strongly support the use of the event-like model in future studies investigating brain activity reflecting sensory pain.

Keywords fMRI, pain, empathy

AALTO-YLIOPISTO
SÄHKÖTEKNIIKAN KORKEAKOULU

DIPLOMITYÖN
TIIVISTELMÄ

Tekijä Tomi Karjalainen

Työn nimi Sensorisen ja havaitun kivun aivomekanismit

Koulutusohjelma Bioinformaatioteknologia

Valvoja Prof. Lauri Nummenmaa

Laitos Lääketieteellisen tekniikan ja laskennallisen tieteen laitos

Ohjaaja Prof. Lauri Nummenmaa

Päivämäärä 12.12.2014 **Sivumäärä** 40 **Kieli** englanti

Tiivistelmä

Diplomityön tarkoituksena oli tarkastella sensorisen ja havaitun kivun aivoverkostoja. Molempien ärsyketyyppien aiheuttamia aivovasteita mitattiin toiminnallisen magneettikuvauksen avulla. Sensorinen kipu aiheutettiin kokeissa johtamalla koehenkilöiden oikeaan jalkaan kipukynnyksen ylittävää lämpöä, kun taas kivuliaita kuvia käytettiin havaitun kivun ärsykkeinä. Kolmea erilaista sensorisen kivun mallia käytettiin yleisen lineaarisen mallin rajoissa. Näistä tapahtumamalli olettaa, että kipuverkostot ovat aktiivisia vain kun jalkaan johdettu lämpötila on kipukynnyksellä tai sen yli, kun taas kaksi muuta mallia, jotka käyttävät pidempiä ikkunafunktioita kipuaistimuksen mallintamiseen, olettavat lisäksi esimerkiksi kivun odottamisen aktivoivan samat kipuverkostot.

Sekä sensorinen että havaittu kipu aiheuttivat voimakasta aivoaktiivisuuden nousua osittain päällekkäisissä, mutta enimmäkseen vierekkäisissä neuronipopulaatioissa molemmilla puolilla aivoja alueella, joka ulottuu pihtipoimun keskiosista avustaville liikealueille. Itse koettu kipu oli tällä alueella lokalisoitunut hieman havaitun kivun aktivaatiokeskuksen takapuolelle. Tämän alueen lisäksi sensorinen kipu aktivoi vasemman tuntoaivokuoren sekä molempien aivosaarien etuosan, kun taas havaittu kipu aktivoi takaraivolohkon laajalti. Käytetyistä malleista tapahtumamallin avulla saadut tulokset ovat aiempien tutkimustulosten kanssa parhaiten yhteensopivia.

Yleisesti ottaen diplomityön tulokset ovat hyvin sopusoinnussa aivojen kipuverkostoihin liittyvän kirjallisuuden kanssa. Niinpä diplomityössä käytetyt koejärjestelyt ja ärsykkeet soveltuvat käytettäväksi myös tuleviin kipututkimuksiin. Työssä havaittuja osittaisia päällekkäisyyksiä aktivoituvissa neuronipopulaatioissa voidaan selittää auttamisen edistämisellä. Sekä saadut tulokset että mallin tulkinnan yksinkertaisuus puoltavat kipuaistimuksen mallintamista tapahtumamallin mukaisesti.

Avainsanat fMRI, kipu, empatia

Preface

The study presented in this Thesis was carried out at PET Centre at University of Turku during the fall semester of 2014. I want to thank my supervisor and instructor Lauri Nummenmaa for arranging me the possibility to complete my degree here in Turku, as well as for his valuable support, guidance and feedback throughout the process. I also want to thank Jetro Tuulari for helping me with data analysis and for offering insightful comments on my work, Lauri Tuominen for both his support and for his resilience as a subject, and Kalle Koskinen and Virva Saunavaara for helping me with the imaging experiments. The help was much needed. Finally, thanks to my family, and especially my parents, for the encouragement and support they have shown throughout my studies, and to my dear Sirpa for being in my life.

Turku, December 12, 2014

Tomi Karjalainen

Table of contents

Abbreviations

ACC	anterior cingulate cortex
BOLD	blood-oxygen-level-dependent
CBF	cerebral blood flow
CNS	central nervous system
EEG	electroencephalography
EPI	echo-planar imaging
FDR	false discovery rate
fMRI	functional magnetic resonance imaging
GLM	general linear model
HRF	hemodynamic response function
LTI	linear and time-invariant
MCC	midcingulate cortex
MEG	magnetoencephalography
MNI	Montreal Neurological Institute
NMR	nuclear magnetic resonance
PAG	periaqueductal gray
PAM	perception-action model
PET	positron emission tomography
PFC	prefrontal cortex
RF	radiofrequency
RVM	rostral ventromedial medulla
STT	spinothalamic tract
T1	longitudinal relaxation time
T2*	transverse decay time
TE	echo time
TR	repetition time

Symbols

Scalars

B_D	magnitude of dynamic magnetic field (T)
E_{mag}	magnetic energy (J)
M	net magnetic moment (J/T)
t	time (s)
γ	gyromagnetic ratio (1/(s·T))
ω	precession frequency (rad)
θ	flip angle (rad)
T_1	longitudinal relaxation time (s)
T_2	transverse relaxation time (s)
σ^2	variance
S_1	pain stimulus function
S_2	warmth stimulus function
S_3	rest stimulus function
Θ	temperature (°C)
Θ_1	noxious temperature (°C)
Θ_2	non-noxious temperature (°C)
Θ_3	rest temperature (°C)
$g(t)$	output of an LTI system
$h(t)$	impulse response of an LTI system
$s(t)$	stimulus function

Vectors and matrices

$\boldsymbol{B} \in \mathbb{R}^3$	magnetic flux density (T)
$\boldsymbol{S} \in \mathbb{R}^3$	spin angular momentum (J·s)
$\boldsymbol{\mu} \in \mathbb{R}^3$	magnetic moment (J/T)
$\boldsymbol{Y} \in \mathbb{R}^{m \times n}$	functional magnetic resonance imaging data matrix with n voxels and m data points (arbitrary unit)
$\boldsymbol{X} \in \mathbb{R}^{m \times p+1}$	design matrix with $p+1$ m-dimensional regressors
$\boldsymbol{A} \in \mathbb{R}^{p+1 \times n}$	matrix consisting of $p+1$ regressor weights for each n voxels
$\boldsymbol{E} \in \mathbb{R}^{m \times n}$	error matrix with zero-mean and Gaussian entries
$\boldsymbol{\varepsilon}_j \in \mathbb{R}^{\boldsymbol{m}}$	random error term for voxel j
$\boldsymbol{I}_{m \times m}$	identity matrix of size m

Operators

$\|\cdot\|$	L^2-norm of a vector
$\mathbb{E}[\cdot]$	expected value

1 Introduction

Sensory pain is an unpleasant sensation whose primary biological purpose is to warn of potential tissue damage. It enables the perceiver to quickly focus attention to the source of the pain, and thus makes it possible for the individual to protect itself. Such protection mechanism has obvious evolutionary benefits. However, not all pain benefit the perceiver. Sometimes the same central nervous system mechanisms that are responsible for the benign effects of pain perception are disturbed, leading to detrimental outcomes, such as chronic pain. More comprehensive understanding of the brain mechanisms underlying the experience of pain is needed to effectively treat such impairments.

Owing to its intense aversive nature, pain is perhaps the simplest sensation to mentally simulate. For example, it is possible for humans to imagine how an injury in someone else would have felt had it happened to the observer, if a video clip of the accident is available. This is an example of empathy. Simulating other individuals' internal states of mind allows people to effectively understand each other (Gallese & Goldman 1998), facilitating sociality. Modern brain imaging technology has enabled investigation of the neural representations of such simulations. Studies conducted on the subject have revealed consistent overlap between the brain circuits activated by directly and vicariously experienced pain (Lamm et al. 2011). The apparent overlap between the neural populations responsible for pain related to self and others has fueled discussion about whether shared neural populations could be the general neuropsychological mechanism underlying empathy (Decety 2011; Bernhardt & Singer 2012; Lamm & Majdandžić 2014). Natural selection favors such multi-functionality: once the neural circuits associated with perceiving pain are in-place, they can be exapted for related purposes with relatively low costs (Darwin 1859, p. 197; Gould & Vrba 1982).

The aim of this Thesis was to study the brain circuits representing sensory and vicarious pain. Previous neuroimaging studies have systematically found that both of these stimulus modalities trigger bilateral activation in the anterior insular cortex and the anterior/midcingulate cortex in addition to the modality-specific regions (Lamm et al. 2011). Experiments with functional magnetic resonance imaging (fMRI) using i) heat-induced pain and ii) pictures of painful feet were conducted to test whether such results could be replicated. Sensory pain was modeled in three different ways within the framework of the general linear model. The event-like model assumes that brain's pain-circuits are specifically activated by noxious stimulus, while the two other models that used long and intermediate blocks

additionally assumed, to different degrees, that also expectation of pain activates the same circuits. Because the brain's pain-circuits are well known, the results of the Thesis were expected to clarify whether the selected equipment, stimuli and data analysis methods could be used, and how they could be developed, to elicit and reveal consistent pain responses in the brain.

The Thesis has two theory chapters. The first of them, Chapter 2, explains the current knowledge regarding the central nervous system mechanisms underlying both sensory pain and empathy. The emphasis is in the brain, as the title of the Thesis suggests. Chapter 3 focuses on the interdisciplinary subject of fMRI: The underlying physics, the neurobiological interpretation of the measured signal along with the controversies related to it, and data analysis using the general linear model are covered. The remaining chapters are devoted to the experimental part of the study: Chapter 4 explains the materials and methods used. The results of the studies are presented in Chapter 5, and they are discussed in Chapter 6.

2 Neural basis of pain and empathy

2.1 Pain

Pain is an essential injury-warning mechanism. People who are congenitally insensitive to pain typically live short lives compared to others because they are prone to hurt themselves (Bennett & Woods 2014). The physiological explanations for pain have evolved significantly since Descartes, who, in the 17th century, famously claimed that a proper peripheral stimulus *necessarily* leads to the perception of pain in the brain (Descartes 1633/2004, pp. 117-118). We now know that the perception of pain is more complex than he supposed. Factors independent of the stimulus, such as attention and previous experiences, are known to affect the perception, suggesting that the central nervous system actively modulates the pain signals entering the brain. This section discusses how the emphasis in pain theories has shifted from the periphery to the brain, and summarizes the current knowledge regarding pain perception.

2.1.1 Peripheral pain physiology

Over a century ago, Sherrington (1903) claimed to have found considerable evidence of nerve-endings specialized to stimuli that injury the skin. Around that time, there were two mutually exclusive theories concerning the physiological mechanisms responsible for the experience of pain. According to the *specificity theory* – that Sherrington argued for – pain is an independent sensation with its own peripheral receptors. In other words, the theory suggests that there are receptors that selectively response to noxious but not to non-noxious stimuli. The *pattern theory*, on the other hand, proposed that the nerve-endings in the periphery are all alike, and that it is the activation pattern of the nerves that determines if the activation is perceived as pain. (Woolf & Ma 2007)

In their classic article, Melzack and Wall (1965) presented the *gate control theory* of pain, which was an attempt to incorporate several independent pain-neurophysiological findings under a single theory. Despite Sherrington's claim several decades earlier, there was little reported evidence for pain-specific fibers at the time, and the gate control theory proposed, instead, that the experience of pain results from a proper activity pattern in large and small peripheral fibers. A few years later, electrophysiological recordings conducted by Bessou and Perl (1969) revealed that i) some unmyelinated C fibers respond to noxious but not to non-noxious stimulus, and ii) that other C fibers respond to non-noxious but not to noxious stimulus. The results strongly supported the specificity theory. Evidence in favor of fibers selectively activated by noxious stimuli started accumulating, and today the pattern theory has

been firmly discarded (Woolf & Ma 2007). Even if some details of the gate control theory proved to be wrong, it included ideas such as central descending control of nociceptive input, which later research has since then found to be an integral factor contributing to pain perception (Mendell 2014).

The free nerve-endings selectively activated by noxious stimuli and postulated by the specificity theory are referred to as *nociceptors*, some of which have a thin myelin sheet around their axons (Aδ-fibers) while most do not (C-fibers). A noxious stimulus (e.g. intense pressure or heat) triggers an action potential along the axon of the nociceptor. Nociceptors synapse at the dorsal horn of the spinal cord, and the signal ascends to the brain in one of at least three different tracts. (Tracey & Mantyh 2007; Willis & Westlund 1997; Besson 1999)

2.1.2 Pain in the brain

Based on evidence from animal studies and spinal cord deficits in humans, three classic ascending pain pathways have been identified: the contralateral spinothalamic tract (STT), spinoreticular tract and spinomesencephalic tract. The STT transmits noxious information to the thalamus, while the spinoreticular and spinomesencephalic tracts terminate at medulla and brainstem. (Tracey & Mantyh 2007) The midbrain terminal sites include, among others, the periaqueductal gray (PAG) and nucleus cuneiformis (Willis & Westlund 1997). The purpose of the tracts depends on their origin in the dorsal horn as well as on their final destination: The projections to brainstem are related to integrating nociceptive information with homeostatic, arousal and autonomic processes. They also provide a way to indirectly transmit nociceptive signals to the forebrain after brainstem processing. (Tracey & Mantyh 2007) Thalamus, on the other hand, acts as the main relay site for the nociceptive signals both to cortical areas, such as somatosensory cortex, as well as to subcortical structures, such as amygdala and hypothalamus (Willis & Westlund 1997; Garland 2012; Tracey & Mantyh 2007). It also has a role in opioid-mediated pain modulation (Wey et al. 2014).

There is substantial overlap between pain-sensitive brain regions that independent neuroimaging research groups have identified, and today the neural circuits related to pain processing are well established (Apkarian et al. 2005; Farrell et al. 2005; Tracey & Mantyh 2007). The activation pattern is usually bilateral, although the contralateral activation is often stronger (Wager et al. 2013). The most consistently observed pain-related areas, illustrated in Figure 1, are often referred to as *pain matrix* (Melzack 1999) which is typically considered to consist of the thalamus, somatosensory, insular and anterior cingulate cortices (ACC) as well as other regions, such as prefrontal cortex (PFC), periaqueductal gray and rostral

ventromedial medulla (RVM). The activity in the pain matrix correlates positively with the perceived intensity of pain (Wager et al. 2004; Tölle et al. 1999; Wager et al. 2013; Baliki et al. 2006), implying a simple pain-associated interpretation for the activity of the network. Another widely recognized feature of the pain matrix is that it comprises affective (e.g. anterior insula and ACC) and sensory (somatosensory areas) components (Melzack 1999; Singer et al. 2004; Bufalari et al. 2007).

Controversy exists about the interpretation of the activity of the pain matrix (see the review by Legrain and colleagues (2011) for a detailed discussion). First, several studies have found that the magnitude of activation in the pain matrix can be distinguished from the intensity of either experienced pain or the stimulus. Second, factors independent of the stimulus intensity – such as novelty of the stimulus – contribute to the intensity of perceived pain. Third, also non-nociceptive stimuli have been found to activate a similar network. These findings led Legrain and colleagues (2011, p. 111) to propose an alternative interpretation for the network. They suggest that the network is *"involved in detecting, orienting attention towards, and reacting to the occurrence of salient sensory events"* instead of being specifically related to pain.

Recent evidence from fMRI studies investigating the issue is contradictory. Mouraux and colleagues (2011) used different stimulus modalities, including auditory, visual and pain, within a similar attentional context: they applied transient stimuli to the right side of the subject. They found *no* evidence for pain-specific brain regions. Rather, they suggest that the pain-induced brain responses reflect mostly multimodal brain processes that are important for many sensory systems. In line with the suggestion by Legrain and colleagues, they argue that the pain matrix has a crucial role in detecting and reacting to salient or behaviorally relevant sensory stimuli. On the other hand, a recent study by conducted by Wager and colleagues (2013) yielded opposite evidence. They used data from a group of participants to identify a pain signature, i.e. a group of voxels whose activation pattern is typical for pain perception, using a machine-learning algorithm. Then, using data from an independent group of participants, they used the identified voxels to predict whether the subjects had perceived pain or warmth during a scan. With classification sensitivity of 93 % and specificity of 95 %, their results strongly argue in favor of pain-specific role of the pain matrix. The contradiction remains one of the open questions in the field.

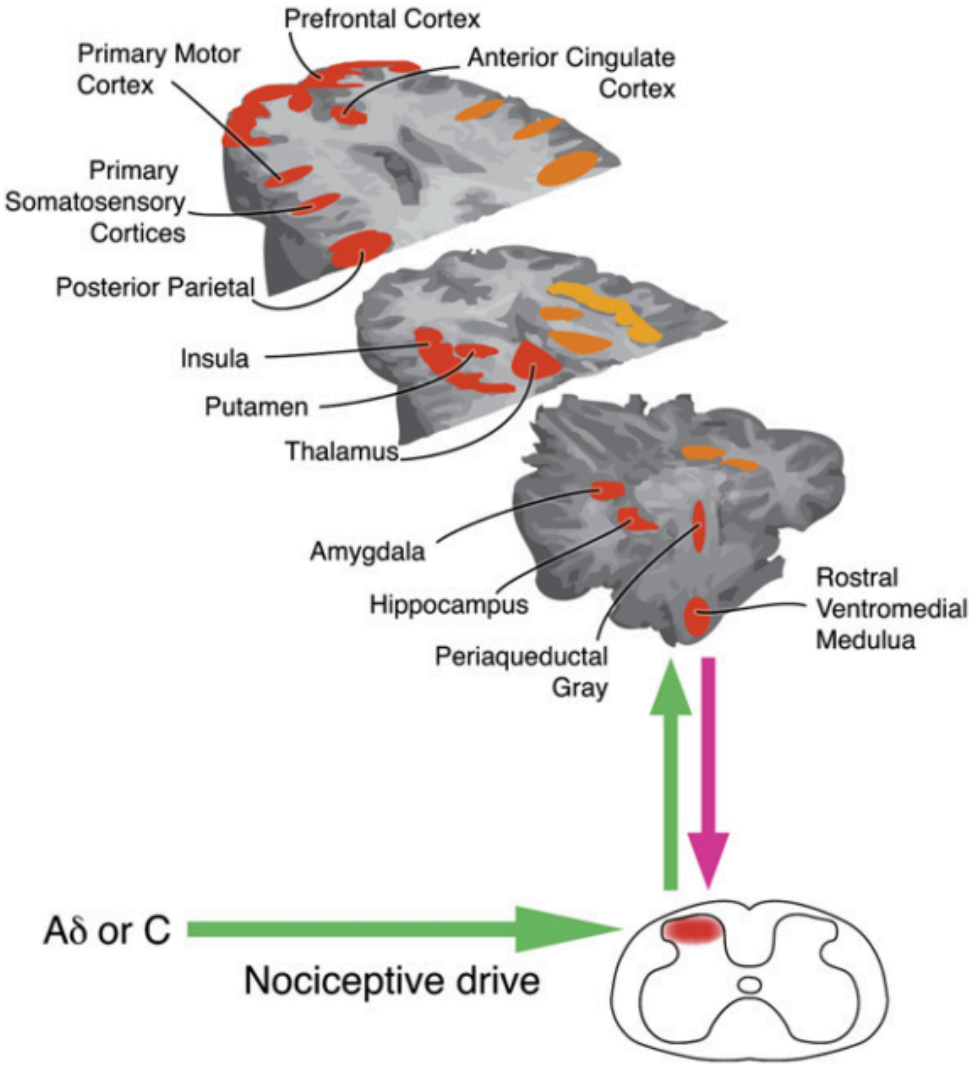

Figure 1. Brain circuits of pain. The areas most consistently activated in pain studies are highlighted in transverse sections of brain. The activation is usually bilateral (red-ipsilateral, orange-contralateral), although the contralateral activity is usually stronger. (Tracey & Mantyh 2007, p. 379).

Factors independent of the nociceptive stimulus can strongly affect the experience of pain. For example, during hyperalgesia stimuli that are normally experienced as non-noxious are perceived as noxious. Also, attending to noxious stimulus increases the level of perceived pain. (Tracey 2010) These phenomena prove that the perception of pain is not fully determined by the physical properties of the stimulus. Thus, the central nervous system must somehow control the pain signals. Considerable evidence exists that some brain regions are actively involved in modulating the nociceptive input entering the brain (Basbaum & Fields 1984; Tracey & Mantyh 2007), explaining the phenomena. The modulation can either facilitate or inhibit the nociceptive transmission (Fields 2004). The regions involved in the control are said to constitute the *descending modulation system* of pain, and it is believed that the purpose of the system is to ensure that the perceived pain is appropriate for the particular circumstance (Tracey & Mantyh 2007).

The brainstem regions PAG and RVM are known to be central components of the descending pain modulation system (Basbaum & Fields 1984; Behbehani 1995). Animal studies have revealed that both regions include descending spinal efferents that can modulate the nociceptive input at the spinal cord level (Reynolds 1969; Mantyh & Peschanski 1982; Basbaum & Fields 1984). Being both a central receiver and a transmitter of noxious information, the PAG allows multiple brain regions to exert their influences to pain perception (Behbehani 1995). It integrates information from frontal cortex, the insula, the amygdala, and the hypothalamus (Basbaum & Fields 1984). Projections from the PAG cover most of the same areas, such as PFC, amygdala, thalamus, hypothalamus and the RVM (Hadjipavlou et al. 2006). RVM is the final site integrating most signals from other regions of the descending modulatory system before outputting the combined information to the dorsal horn (Gebhart 2004; Tracey 2010). Apart from the projections via the RVM, there are also descending projections from the PAG directly and indirectly through the dorsolateral funiculus to the dorsal horn (Behbehani 1995), allowing the PAG to modulate the noxious signals independent of the RVM.

2.2 Empathy

In a broad sense, empathy is related to one person being affected by another's emotional or arousal state (de Waal, 2008). Empathy enables humans – as well as many other animals – to quickly recognize the emotional states of others, promoting understanding that is an important part of sociality. Wealth of evidence suggests that shared neural representations for direct and vicarious experiences of affective states underlie empathy (Bernhardt & Singer 2012). This section discusses the idea of shared representations, introduces the mirror neuron system, speculates about the possible link between these two ideas, and explains how pain research has already contributed to the current knowledge about empathy.

2.2.1 Shared neural representations

In their influential theoretical review, Preston and de Waal (2002) argued in favor of the *Perception-Action Model* (PAM) of empathy. The model states that perception of the attended individual's emotional state automatically activates the observer's neural representations of the state, along with the autonomic and somatic responses associated to it. In other words, detecting and recognizing a feeling in others triggers a neural activity pattern that would produce the same feeling in the observer. This, in turn, helps the observer to understand the other person's intentions. Similar psychological mechanism underlying empathy was suggested by Gallese (2003). The theory of shared representations has become the dominant

approach to understanding the mechanisms responsible for empathy (Singer & Lamm 2009; Bernhardt & Singer 2012).

A possible candidate as the neurophysiological explanation for the shared neural representations is *the mirror neuron system* (Iacoboni 2009). First discovered in monkeys and later in humans, mirror neurons are a particular class of neurons in frontal and parietal areas that activate both during an action and the observation of the same action (di Pellegrino et al. 1992; Rizzolatti & Craighero 2004; Mukamel et al. 2010). The discovery of mirror neurons has revealed that the motor system has a role in understanding others in addition to controlling movements (Ferrari & Rizzolatti 2014). Indeed, mirror neurons have been proposed to be responsible for action understanding as well as mediating imitation (Rizzolatti & Craighero 2004; Nishitani & Hari 2000). Recent findings support their causal role specifically in action understanding (Michael et al. 2014).

Both imitation and action understanding are closely linked to empathy. It is therefore not surprising that mirror neurons are a popular candidate as a neural substrate contributing to empathy. It has been suggested that empathy is implemented in the brain by simulating the mental states of others, and that mirror neurons provide an automatic mechanism for the simulation (Gallese & Goldman 1998; Singer & Lamm 2009; Iacoboni 2009). An important study supporting this theory was conducted by Carr and colleagues (2003). In the study, the subjects were shown pictures of facial emotional expressions that they were instructed to either observe or imitate. They investigators found a large network consisting of i) the mirror neuron system, ii) the limbic system, and iii) the insula, that connects these two systems, to be actively involved in both conditions, and argued that this overlap is a sign of empathy. The results of the study can be interpreted in a way that is perfectly consistent with the idea of shared representations: The mirror neuron activity supports the simulation of the observed facial expression, which triggers activity in the limbic system through the insula, producing the observed emotion (Iacoboni 2009).

Even if mirror neurons might contribute to empathy via mirroring motor activity, people can also empathize with others purely cognitively, that is, without direct sensory stimulus such as facial expression of an emotion, but rather only on the basis of a story. Consequently, mirror neurons cannot be the only neurophysiological mechanism underlying empathy. The so-called mentalizing network – including medial PFC, the temporo-parietal junction and the medial parietal cortex (Mitchell 2009) – has been suggested to be responsible for the more cognitive

component of empathy, thus complementing the mirror neuron system in enabling empathy. (Bernhardt & Singer 2012)

2.2.2 Empathy for pain – evidence for shared representations

Observing others in pain often feels unpleasant or even painful and thus can motivate the observer to help the other (Hein et al. 2010). This is a prime example of empathy in use and the shared aversiveness suggests, perfectly in-line with the PAM, that the same neural circuits that are associated with perceiving pain are also activated in the observer.

Neuroimaging studies of empathy have extensively used pain to induce the emotion (Singer et al. 2004; Lamm et al. 2011; Corradi-Dell'Acqua et al. 2011; Bufalari et al. 2007). Two types of paradigms have been typically used. In the first paradigm, the subjects are shown painful visual stimuli (pictures or videos). In the second paradigm, a visual cue informs the subject that someone else, usually a person close to the subject, is experiencing pain.

Using the cue-paradigm, Singer and colleagues (2004) found that empathy for pain involves only the affective and not the sensory dimension of the pain matrix. Similar results have been obtained also using the visual-paradigm (Jackson et al. 2005; Botvinick et al. 2005). These initial results suggested that only the emotional representations of pain are shared. However, later studies found that observing someone else's pain can also activate the sensorimotor components of the pain matrix (Botvinick et al. 2005; Lamm et al. 2007; Avenanti et al. 2005). In their review, Singer and Lamm (2009) suggest that the salience of the somatosensory quality of pain determines whether the sensory components of the pain matrix are activated or not: moderate pain only activates the motivational and affective components, while more intense pain additively triggers activity in the sensory parts of the matrix. Corradi-Dell'Acqua and colleagues (2011) used multivariate pattern analysis on fMRI data to study the hypothesis of shared representations for vicarious and sensory pain. They found evidence for shared patterns of neural activity in bilateral anterior insula, right middle insula and midcingulate cortex, and suggested that middle insula and midcingulate cortex share information specific to pain, while the anterior insula shares information related to the associated emotional effects.

Importantly, these studies and many others reveal consistent overlap between brain circuits activated by vicariously and directly experienced pain. To validate the consistency, Lamm and colleagues (2011) did a meta-analysis on the subject. They found that the anterior insula and the medial/anterior cingulate cortex have been systematically associated with empathy for

pain, regardless of the paradigm used. These areas are also consistently activated during firsthand experience of pain. It is exactly this kind of overlap between regions associated with vicarious and sensory pain that has been interpreted as strong evidence for shared neural representations underlying empathy.

Despite the consistent overlap between brain regions activated by directly and vicariously experienced pain, it must be noted that the extent of the voxel-to-voxel overlap is rather small. The activation loci within the insula and ACC for self-related pain are systematically more posterior compared to others-related pain activity. (Jackson et al. 2006) In addition, as most of the results have been obtained using fMRI, whose spatial resolution is insufficient for tracking activity from individual neurons, it is possible that distinct but neighboring neural populations associated with self vs. others –related pain exist even within the overlapping voxels in the brain. (Singer & Lamm 2009)

As the PAM predicts, the neural representations of firsthand pain and empathy for pain are, at least partly, shared. What is the neurobiological explanation for this? There is currently no evidence of mirror neurons existing in insular or cingulate cortex. Neither does the mentalizing network include these areas. One possible explanation for the observed similarities is that the endogenous opioid system is engaged in both conditions. Opioids are neurotransmitters that are perceived as analgetic and pleasant. They are released during pain-perception (Zubieta et al. 2001; Wey et al. 2014), and their original biological role is probably in pain modulation. Importantly, the PET-study conducted by Zubieta and colleagues (2001) showed that opioids are released significantly in both anterior insula and midcingulate cortex during pain perception. As numerous fMRI studies have identified these same brain regions to be also activated during empathy for pain, could the opioid system also contribute to empathy? The opioid system is known to play an important role in modulating animal social behavior (Machin & Dunbar 2011), suggesting that the opioid system really was exapted for sociality purposes at some point during evolution. However, there is no direct evidence of the endogenous opioid system's role in human sociality, or more specifically, empathy. Thus, no reliable conclusions about the theory can be made.

This Thesis serves as a preparation for a research project investigating the endogenous opioid system's role in human sociality. Empathy for pain will be aroused using painful pictures, while noxious heat is used to induce sensory pain. Dynamic brain activity reflecting these conditions will be measured using fMRI. The following Chapter explains how fMRI can be used for indirectly measuring brain activity.

3 Functional magnetic resonance imaging

Modern cognitive neuroscience relies heavily on the use of fMRI. In anatomical MRI, the aim is to create a maximal contrast between different body tissues, whereas fMRI measures brain function. Compared to other functional brain imaging techniques such as electroencephalography (EEG) and magnetoencephalography (MEG) whose signals have a rather straightforward neurophysiological interpretation, variation in the fMRI signal is mostly explained by changes in cerebral blood flow (CBF) and the oxygenation level of the blood. These variables do not directly reflect neural activity, but are merely correlated with it.

The chapter begins with an introduction to nuclear magnetic resonance (NMR), the physical phenomenon that is central to understanding MRI. The reader is presented with the basic mechanisms of signal transmission in the nervous system. The third section is devoted to explaining how the fMRI signal can be used to convey information about neuronal activity. Finally, the statistical analysis of fMRI data using general linear model is explained.

3.1 Principles of nuclear magnetic resonance

Many atomic nuclei, such as that of hydrogen, have magnetic properties that are revealed by their interactions with static and dynamic magnetic fields. The following subsections give physical explanations for the interactions, as well as explain the MR image formation.

3.1.1 Nuclear spin and magnetic moment

One of the key concepts in NMR physics is the *spin*. It is an intrinsic property of an elementary particle in the same way as mass and electric charge are to electrons. Spin is a highly abstract quantum-mechanical concept that is often conceptualized as the intrinsic rotation of a particle around its own axis. In NMR context, it is more convenient to talk about spins of atomic nuclei instead of single particles. Most atomic nuclei, including that of hydrogen's, have spin. Spin $\boldsymbol{S}$ is a form of angular momentum and it is related to the magnetic moment $\boldsymbol{\mu}$ via the equation

$$\boldsymbol{\mu} = \gamma \boldsymbol{S}, \tag{1}$$

where the nucleus-specific scalar γ is known as the gyromagnetic ratio. It is positive for most nuclei, and thus the magnetic moment and spin are parallel. If a spin particle is exposed to an external magnetic field **B**, its magnetic energy depends on the angle between the magnetic moment $\boldsymbol{\mu}$ of the particle and the magnetic field:

$$E_{mag} = -\boldsymbol{\mu} \cdot \boldsymbol{B}. \quad (2)$$

According to Equation (2), the lowest energy state is reached when the magnetic moment is parallel to the external magnetic field. This has important consequences.

A group of spin particles form a spin system. In MRI, the imaged tissue is divided into distinct small cubes called voxels. In this context, a convenient spin system could consist of all the hydrogen nuclei within a single voxel. The sum of all magnetic moments in such system defines the net magnetization of the system. Under normal conditions (temperature and magnetic field) on Earth, the magnetic moments of the individual elements of the spin system are uniformly distributed in space. Thus, the net magnetization is essentially zero. To reveal the net magnetization of the system, it has to be exposed to static magnetic field. (Levitt 2008)

3.1.2 Effect of static magnetic field on spin systems

At macroscopic scale, when a magnetic moment is exposed to an external static magnetic field, the field forces the magnetic moment to align parallel to it. A compass is a familiar example of this. A spin particle exposed to a static external magnetic field, on the other hand, does not align with the magnetic field but starts *precessing* about it, as in Figure 2. Precession angle is determined by the orientation of the spin axis at the moment the external magnetic field is applied. (Levitt 2008) In MRI, the static magnetic field is constantly on, and the individual spins exposed to the field are thus continuously precessing.

Figure 2. A spin particle (black arrow) precesses about the axis determined by the external static magnetic field (white arrow). (Levitt 2008, p. 27)

The rate at which the spin precesses is known as the *Larmor frequency*. It is proportional to the magnitude of the external magnetic field, with the gyromagnetic ratio acting as the scaling constant:

$$\omega = -\gamma \|\boldsymbol{B}\|. \quad (3)$$

Nuclei are surrounded by a large quantity of other nuclei and molecules that act as sources of dynamic magnetic fields. For each particle in the system, the dynamic magnetic fields are different. Since the sum of the static and dynamic magnetic fields determines the precession axis, the magnetic moments of the spin particles start slowly wandering around. Because of finite temperature, the most probable orientation for any magnetic moment in the system is along the minimum energy direction, that is, parallel to the static magnetic field. This causes a gradual breakdown of the initial orientation uniformity, and leads to a stable net magnetization component along the static magnetic field, revealing the magnetic properties of the system, as illustrated in Figure 3.

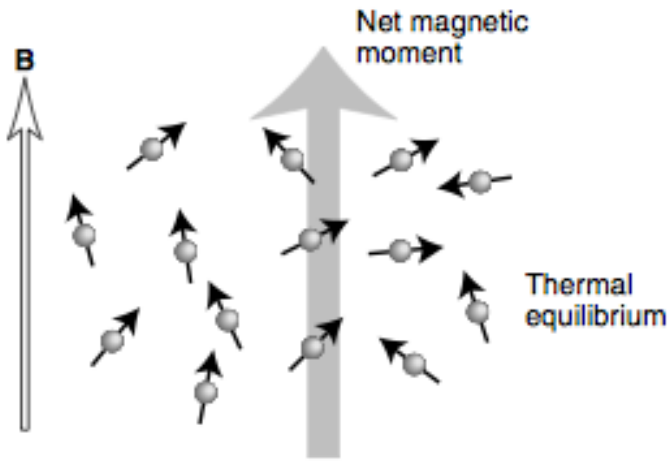

Figure 3. External static magnetic field (B) causes a spin system to align the net magnetization vector with it. (Levitt 2008, p. 32)

Assume that the static magnetic field is applied along the z-axis at time t_{on}. Then the build-up of the net magnetization along the axis is described by the equation

$$M_z(t) = M_z^0(1 - e^{-\frac{t-t_{on}}{T_1}}), \tag{4}$$

where M_z^0 is the initial net magnetization. The parameter T_1 determines how quickly the system stabilizes. It is tissue-specific, which allows creating a contrast between different tissues, such as bone and brain. In MRI, the static magnetic field is typically defined from feet to head.

3.1.3 Effects of dynamic magnetic fields on spin systems

Exposing a spin system to a static magnetic field creates a net magnetization along the direction of the magnetic field. Unfortunately for MRI, the magnetization is difficult to

measure since it is parallel to the magnetic field that is significantly larger in magnitude. Thus, the magnetization has to be rotated so that it is no longer fully parallel to the static magnetic field. In MRI, the spin system whose net magnetization is rotated consists of a slice of voxels. This guarantees that the signal that is eventually measured originates from the slice.

Dynamic magnetic fields B_D, oscillating at the Larmor frequency of the atomic nucleus of interest, can be used to rotate the net magnetization. The fields are applied in short radiofrequency (RF) pulses, usually having a form of sinc function that has a uniform spectrum over a specified frequency interval (Jezzard & Clare 2002, p. 78). The RF pulses affect the spin system in two ways. First, they provide energy to the system so that the number of high-energy spins increases, effectively decreasing the magnitude of the z-component of the net magnetization. Second, the pulses cause the spins to precess more coherently, increasing the magnitude of the transverse component. It can be shown that applying an RF pulse for t seconds rotates the net magnetization

$$\theta = \gamma B_D t \tag{5}$$

radians (Huettel et al. 2008, p. 82), which is called the *flip angle*. For any given flip angle, the required duration of the pulse can be calculated from the Equation (5). Typically, MR imaging uses a flip angle of 90° because this maximizes the net magnetization component perpendicular to the static magnetic field.

3.1.4 Relaxation mechanisms

Once the RF pulse ends, the rotation of the net magnetization ends. The new orientation is not stable, and the magnetization starts gradually returning to its initial position parallel to the static magnetic field according to the Equation (4). This phenomenon is called *longitudinal relaxation.* How much the magnetization is allowed to recover in MRI is described by repetition time (TR), which is defined as the time between two successive RF pulses. Long TRs allow maximal signal-to-noise ratio but increase the duration of the measurements as well as decrease the temporal resolution.

The reduction in the component perpendicular to the static magnetic field, which is called the transverse component, decreases simultaneously with the longitudinal component as the RF pulse ends. The decrease obeys equation

$$M_{xy}(t) = M_{xy}^0 e^{\frac{-t}{T_2}}, \tag{6}$$

where T_2 is a time-constant that determines the rate of the decay. The theoretical explanation for the T_2 decay is that the magnetic moments that were rotated to the transverse plane lose their initial phase coherence due to spin-spin interactions. Another source contributing to the decay is that the magnetic field is never fully homogeneous. Due to the small inhomogeneities in the field, the spins precess at slightly different rates as Equation (3) predicts, contributing to the incoherence. The transverse decay resulting from the combination of spin-spin interactions and magnetic field inhomogeneities is known as T_2^* decay. (Huettel et al. 2008, p. 66) Like T_1, also T_2^* is tissue-specific (Chavhan et al. 2009). Importantly for MRI, signal can only be measured as long as the magnitude of the transverse magnetization is significant enough. Thus, the constant T_2^* determines the length of the time window during which measurements can be made.

3.1.5 Image reconstruction

Once a spin system has been exposed to an RF pulse, the net magnetization of the system has a precessing component perpendicular to the static magnetic field. The magnetic moment acts as a source of a magnetic field. As the magnetic moment rotates, the magnetic flux through the detector coil changes, which, according to the Faraday's law, induces a voltage and current in the coil. (Levitt 2008) This is the main principle underlying MR signal acquisition. Critically, the measured current carries information about the frequency composition of the precessing spin system, permitting reconstruction of an MR image.

Reconstructed MR images – both anatomical and functional – are three-dimensional matrices whose entries represent the intensity of the signal in the corresponding voxel. Typical voxel size in fMRI is 2 mm x 2 mm x 2 mm. There are no individual receiver coils for each voxel. Instead, only one coil is usually used. Thus, the MRI scanner has to be able to spatially encode the signal in a way that enables tracing the contribution of each voxel to the measured signal. The spatial encoding is done in three steps: slice selection, phase encoding and frequency encoding.

The images are acquired as sequences of two-dimensional slices. That is, an RF pulse activates a single slice within the tissue of interest. This is called slice selection. Slice selection is accomplished by transiently superimposing a magnetic field gradient along z-axis (e.g. negative values for negative z-coordinates and positive for positive z-coordinates) on the static magnetic field. Due to the gradient, the residual magnetic field strength – and the Larmor frequency along with it – is determined by the z-coordinate of the system. Thus, by

transmitting RF pulses oscillating at properly chosen frequency bands while the gradient is on, desired slices can be selectively activated (Jezzard & Clare 2002, p. 78).

After slice selection, the phases of the precessing spins within the activated slice are in coherence, and thus, the net magnetization is rotating in the transverse plane. In addition, because the magnetic field that the system is exposed to is static, also the precession frequency is the same for every voxel within the slice. Thus, even if measuring signal from such system is possible, the signal, if measured, would contain no information about the within-slice spatial origins of the signal.

In fMRI, within-slice spatial encoding is often performed using an echo-planar imaging (EPI) sequence (Mansfield 1977). It sequentially introduces two more gradients. The first gradient is applied along the y-axis before the data acquisition period. While the gradient is on, the precession frequencies of the spins are determined by their y-component, causing phase incoherence along the direction of the gradient. Once the gradient has been turned off, the spins have a phase that is determined by their y-coordinate. By introducing the second gradient along the x-axis, the precession frequencies along the axis can be controlled. This is called frequency encoding. During the frequency encoding, the combination of precession frequency and phase is unique for each voxel's net magnetization. Data is acquired during the frequency encoding to take advantage of that. The sequential application of phase and frequency gradients has to be repeated multiple times in order to provide sufficient amount of data for reconstructing an image.

An EPI sequence that is applied to a slice with 64 x 64 voxels lasts approximately 30 milliseconds. Such speed allows the full-brain scanning in approximately 2 seconds. This is much faster than anatomical imaging. The cost of the increased speed is decreased spatial resolution. (Jezzard & Clare 2002, p. 84)

3.2 Blood oxygenation level dependent signal as a measure of neural activity

Pioneering research conducted by Ogawa and colleagues (1990) led to the discovery that blood-oxygenation can be used as a contrast in MRI. The level of oxygen in the blood, it is supposed, can be used as a correlate of neural activity. This section is devoted to discussing the origins of the fMRI signal.

3.2.1 Signal transmission in the brain

The brain tissue consists of two types of cells: glia cells and neurons. Glia cells have an important role in supporting neurons both structurally and functionally, and they form the majority of brain tissue. Neurons, on the other hand, are the information processing units of the brain. Structurally, the most important parts of neuron are the soma, dendrites, the axon and axon terminals. Soma is the center of a neuron and it contains, for example, the nucleus and mitochondria that supply energy for the cell. Dendrites branch out from the soma to form an extensive network. They provide other neurons more area to contact to, and neurons often output their signals to dendrites of other neurons. Information flows in a neuron typically from a dendrite to the soma, and from there via the axon to the axon terminals. Axon is a long projection of nervous tissue from the soma that conducts electrical impulses along it, branching extensively. The numerous end-points of axon are called axon terminals. They typically form synapses with dendrites of other neurons. (Tortora & Derrickson 2008, pp. 450-454)

Neurons have a cell membrane surrounding them. It has a significant role in information processing. Complex proteins called channels and pumps selectively transfer ions through the membrane. The channels and pumps help the cell to maintain both electrical and chemical gradients over the membrane. The electrochemical gradient enables information transmission within a neuron using passive electrical impulses from dendrites to soma and from there as an action potential along the axon to the axon terminals. In most synapses, neurotransmitters are responsible for transmitting the signal to the postsynaptic neuron. Neurotransmitters are molecules that are stored within neurons. When an action potential arrives to axon terminal, the neurotransmitters exit the neuron and diffuse over the synaptic cleft and bind to neurotransmitter-specific receptors in the cell membrane of the postsynaptic cell. As a consequence, ions flow inside the postsynaptic neuron. If the ions are positive, they increase the electrical potential over the membrane, triggering a new electric pulse towards the soma. If the sum of all the nerve pulses reaching the soma is high enough, a new action potential is triggered towards the axon terminals. (Tortora & Derrickson 2008, pp. 458-474)

Using rodent brain, it has been estimated that action potentials and postsynaptic potentials are responsible for up to 80 % of the energy consumption of cells in grey matter (Attwell & Laughlin 2001). Even if the energy production, i.e. the synthesis of adenosintriphospate (ATP), occurs inside the cells in mitochondria, synthesizing ATP requires glucose and

oxygen. Both molecules have to be carried in blood from outside the cells. That considered, it is no surprise that CBF has been observed to strongly correlate with metabolic activity (Hoge et al. 1999; Fox & Raichle 2007; Chaigneau et al. 2007). CBF-increases related to information processing are at the core of fMRI signal, which is covered in the next section.

3.2.2 BOLD-contrast

Figure 4 presents the traditional view of the chain of events leading from neuronal activity to observed blood-oxygen-level-dependent (BOLD) contrast. The association between neuronal activity and increase of CBF has been known for a long time (Roy & Sherrington 1890; Fox & Raichle 2007). Traditionally it was thought that fall in oxygen or glucose concentration would trigger the increase in blood flow. However, this view has been challenged, and mechanisms responsible for the neurovascular coupling are still actively researched (Hillman 2014; Attwell et al. 2010).

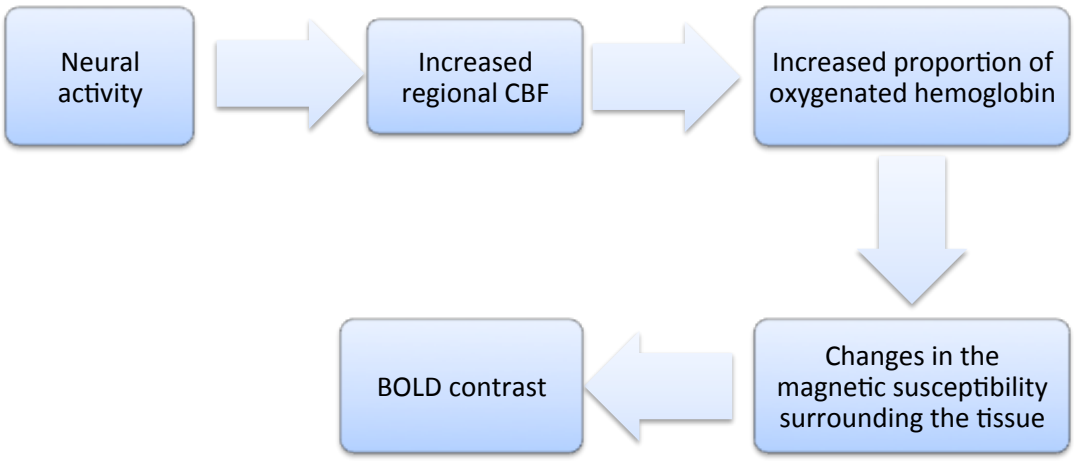

Figure 4. The chain of events linking neural activity to BOLD contrast.

Even if metabolic activity consumes oxygen, it has been observed that the increased CBF overcompensates the consumption, leading to an *increased* proportion of oxyhemoglobin in the blood in metabolically active regions (Malonek & Grinvald 1996). Further, oxy-hemoglobin is known to be diamagnetic, while deoxyhemoglobin is paramagnetic (Pauling & Coryell 1936). Because the oxygenation of hemoglobin has such large effects on the magnetic susceptibility of the molecule, blood-flow alterations change the magnetic susceptibility of the tissue surrounding the blood vessels with increased CBF. Consequently, the magnetic field that the nearby hydrogen nuclei are exposed to changes, affecting their Larmor frequencies. By carefully selecting the oscillation frequencies of the RF pulses, only the hydrogen nuclei

around diamagnetic tissue are excited. This way, the brain's spatial magnetic susceptibility distribution can be interpreted as a BOLD contrast. Ogawa and colleagues (1990) showed that it is possible to produce a functional MRI based on BOLD contrast.

The exact interpretation of the BOLD contrast has been speculated now more than twenty years. An important step in the process was the finding by Logothetis and colleagues (2001). They found that local field potentials recorded using extracellular microelectrodes correlate with BOLD fMRI responses more strongly than single-unit or multi-unit spiking recordings, and concluded that observed neural activation is more likely to result from incoming input currents and their local processing rather than action potentials. A recent study with simultaneous fMRI-PET showed that pain-induced fMRI signal-increase in thalamus is largely explained by decrease in regional opioid receptor binding potential, suggesting that the neurotransmission of opioids was the main contributor to the fMRI signal (Wey et al. 2014), in line with the conclusions made by Logothetis and colleagues. However, neuronal activity is not the only factor affecting the BOLD contrast. All hemodynamic changes, including blood-flow changes not related to information processing, cause similar signals. Thus, despite the popularity of fMRI in research use, the origins of the signal are still rather controversial (Hillman 2014).

3.2.3 Hemodynamic response

The observed BOLD signal that is seen after a short stimulus is known as the hemodynamic response (HDR). Its idealized shape is illustrated in Figure 5. Such idealizations do not exist in reality. However, the idealization has an important role in data analysis that is covered in Section 3.3. HDR typically begins 1–2 seconds after the stimulus onset. In the beginning, the intensity of the signal increases nearly linearly, reaching the peak at approximately 5 seconds after the stimulus. After reaching the peak, the curve falls slowly, usually *undershooting* below the initial baseline. (Huettel et al. 2008, pp. 208)

A longer stimulus and a sequence of consecutive stimuli trigger a response where the short peak is replaced with a longer plateau. Even if this observation suggests linear additivity of the responses for a prolonged stimulus (Boynton et al. 1996), the brain responses are known to also exhibit significant nonlinear behavior (Friston et al. 2000). However, most today's fMRI data analysis software assume the HDR to add linearly due to the simplicity and efficiency of the resulting computations.

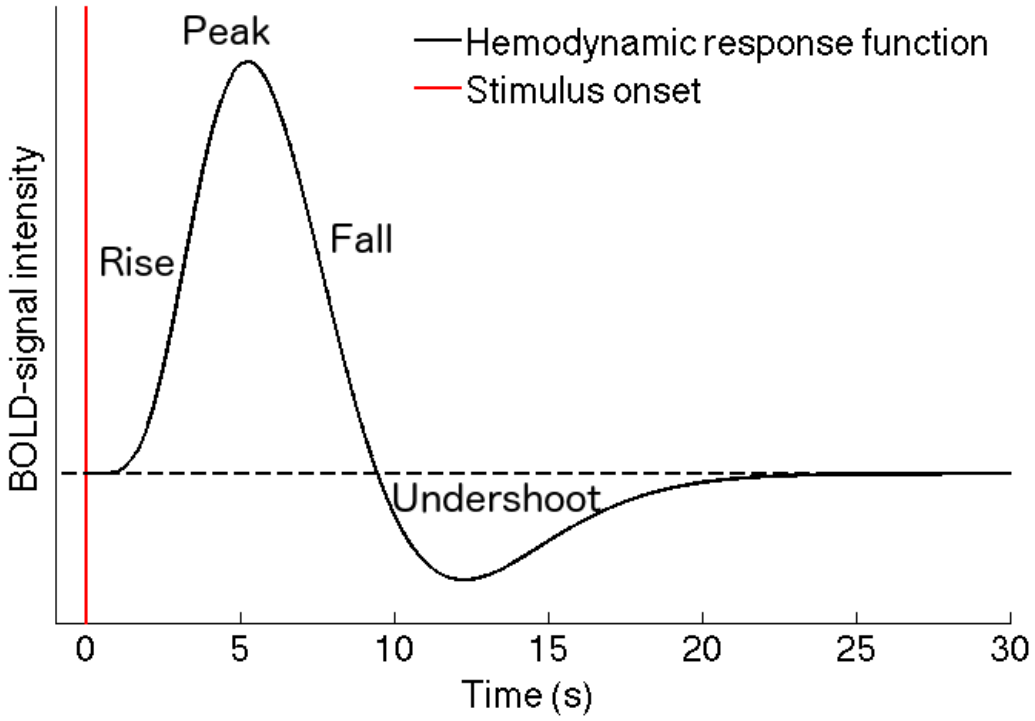

Figure 5. Shape of a canonical hemodynamic response function.

3.3 Data analysis with the general linear model

The most common fMRI data analysis techniques are based on the general linear model (GLM), a classic statistics method that models an independent variable as a linear combination of several dependent variables and an additive random error term. This section briefly introduces the reader to the model and explains how it is used in fMRI to find voxels significantly activated by stimuli.

3.3.1 Specifying the model

In fMRI, the independent variables of the GLM are the time-series of each voxel, and the model can be conveniently written in a matrix form (Friston et al. 1995). Given n voxels and m data points for each voxel, the model can be stated as

$$\boldsymbol{Y} = \boldsymbol{X}\boldsymbol{A} + \boldsymbol{E}, \tag{7}$$

where $\boldsymbol{Y} \in \mathbb{R}^{m \times n}$ is a data matrix whose columns correspond to the time-series of the voxels, $\boldsymbol{X} \in \mathbb{R}^{m \times p+1}$ is the so-called *design matrix* with p regressors as its columns (in addition to a constant vector consisting of ones), $\boldsymbol{A} \in \mathbb{R}^{p+1 \times n}$ includes the voxel-specific parameter weights as its columns, while the columns of $\boldsymbol{E} \in \mathbb{R}^{m \times n}$, denoted here by $\boldsymbol{\varepsilon}_j \in \mathbb{R}^{\boldsymbol{m}}$, are random variables assumed to have the following properties (Huettel et al. 2008, pp. 356):

1. $\mathbb{E}[\boldsymbol{\varepsilon}_j] = \boldsymbol{0}$ for each $j = 1, \ldots, n$ (zero-mean),

2. $\mathbb{E}\left[\boldsymbol{\varepsilon}_j \boldsymbol{\varepsilon}_j^T\right] = \sigma^2 \boldsymbol{I}_{m\times m}$ for each $j = 1, \dots, n$ (homoscedasticity and uncorrelatedness within error terms),
3. $\mathbb{E}\left[\boldsymbol{\varepsilon}_j^T \boldsymbol{\varepsilon}_k\right] = 0$ for each $k \neq j$ (uncorrelatedness between error terms),
4. $\boldsymbol{\varepsilon}_j \sim N(\boldsymbol{0}, \sigma^2 \boldsymbol{I}_{m\times m})$ for each $j = 1, \dots, n$ (normality).

The last assumption is not required in parameter estimation, but it is necessary for assessing the statistical significance of the estimation. Normality also implies that the assumptions of uncorrelatedness are equal to assuming the error terms to be independent.

GLM can be used for identifying voxels that showed statistically significant BOLD-signal changes in response to a regressor of interest. In single-subject analysis, preprocessed data $\boldsymbol{Y}$ and user-specified design matrix $\boldsymbol{X}$, incorporating the selected regressors, are used to estimate the parameter matrix $\boldsymbol{A}$. Least-squares estimation is typically used. (Friston et al. 1995) Large absolute value of a parameter implies a good fit of the corresponding regressor to the measured signal. However, the regressor weights themselves are not often interesting. Rather, researchers use *contrasts* that are defined as a difference between two weights. For example, this Thesis investigates the contrast 'painful – painless' in the vicarious pain experiment. If least-squares estimation is used, the null hypothesis claims that the contrasts are zero-mean Gaussian random variables (Kiebel & Holmes 2006, p. 105). Thus, large contrasts imply violations of the null hypothesis, that is, significant differences between the conditions.

Most studies today use multiple subjects to infer something about the population of interest. At the end of the first-level analysis, there are multiple realizations of a contrast for each voxel. The statistical significance of the first-level estimates can be assessed by using one-sample *t*-test, resulting in a single test statistics for each voxel. Because of the large number of voxels in a typical fMRI study, an important step is to correct for the problem of multiple comparisons. After the correction, the statistics are typically color-coded and superimposed on an anatomical image to visualize which voxels exhibited statistically significant differences between the investigated conditions.

3.3.2 Creating regressor functions

The selection of a proper set of regressors is arguably the most important part of the analysis. As was discussed in Subsection 3.2.3, the hemodynamic response has been observed to have some properties resembling those of an impulse response of a linear system (Boynton et al. 1996). The GLM takes advantage of this by utilizing well-known results from theory of linear

and time-invariant (LTI) systems. If the hemodynamic response function (HRF), such as the one shown in Figure 5, is assumed to be the impulse response function $h(t)$ of an LTI system, then the output $g(t)$ of the system for any stimulus $s(t)$ is obtained by convolving the stimulus with the HRF (Worsley 2002, p. 251):

$$g(t) = \int_0^\infty h(\tau)s(t-\tau)\,\mathrm{d}\tau. \quad (8)$$

The stimulus function is an indicator function with ones during stimuli and zeroes otherwise. The convolution smoothens and delays the stimulus function, mimicking the underlying hemodynamic system. The predicted output of the system can be used as a regressor in the design matrix. (Huettel et al. 2008, pp. 345-352)

The LTI-connection is essential for understanding the creation of the regressors. However, the presented method is slightly simplified, and is typically not used as such in today's analysis software. For example, the model described by the Equation (8) assumes that the HRF is trial-independent, when in fact, it has been observed that the hemodynamic response is not fixed (Friston 1995). To resolve the issue, a fixed HRF can be replaced with basis functions (e.g. gamma functions), allowing stimulus-specific HRFs (Friston et al. 1998). Further, instead of using fixed function parameters, they can be estimated from the data (Lange & Zeger 1997). These computational details do not, however, change the basic idea behind regressor design.

All factors that are known to contribute to the measured signal should be incorporated into the design matrix, unless they are compensated for in the pre-processing stage. Otherwise, those factors contribute to the error terms, which is undesired for several reasons. For one, the error terms are assumed to be zero-mean, and second, they are assumed to be normal, implying a symmetric distribution. Both of these assumptions are likely to be violated if a systematic error source is present but left unmodeled. In addition, unmodeled sources contribute to the error variance, reducing the sensitivity of statistical analysis. As an example of signal sources with no direct experimental interest, head-motion-related artifacts often contribute significantly to the signal. Thus, three regressors are usually used to account for translational movements and additional three are used for rotations. However, even if increasing the number of nuisance factors might be appropriate because of the assumptions of the GLM, every additional regressor reduces the degrees of freedom by one, decreasing the sensitivity of statistical inference. Thus, the selection of each regressor has to be properly justified. (Huettel et al. 2008, pp. 349)

4 Materials and methods

The study investigated the differences and similarities between fMRI activity patterns in response to sensory and vicarious pain. Foot-localized heat was used to induce sensory pain, while pictures of painful feet were used as the stimuli for vicarious pain. In both experiments, the stimuli were presented and controlled using Presentation (Neurobehavioral Systems).

4.1 Subjects

There were 6 subjects with 2 women (mean: 30.1 years; SD 4.1 years). All the subjects were volunteers from within the laboratory.

4.2 Experimental design

4.2.1 Sensory pain

The 'pain localizer' experiment conducted by Corradi-Dell'Acqua and colleagues (2011) was replicated with slight modifications. Noxious and non-noxious heat localized to the right foot (medially) was delivered using a computer-controlled thermal stimulator with an MRI-compatible (50 mm x 50 mm) fluid-cooled Peltier probe (MSA Thermotest). The non-noxious temperature was 37 °C while the noxious temperature was subject-specific. A rest temperature of 32 °C was used.

Pain threshold measurements before the session were conducted to select the noxious temperature. Ascending method of limits was used: starting from 25 °C, the temperature increased slowly (1 °C/s) until subject's response, indicating that the temperature was sufficiently strong to be considered painful but sufficiently weak to be felt without moving the foot. The measurement was repeated five times, and the average of the last four measurements, rounded to one decimal accuracy, was then used as the noxious temperature during the actual experiment. The noxious temperature ranged between 44.8…49.3 °C (mean: 47.58 °C; SD: 1.92 °C).

The graph shown in Figure 6 illustrates the alternating pattern of noxious and non-noxious stimuli that was used in the experiment. The stimuli were delivered in 10 double-blocks (each 24 second-long): five blocks with noxious temperature alternated with five blocks with a non-noxious temperature. The blocks were separated by a rest interval of 24 s during which the temperature was fixed to 32 °C. Each block was organized into two consecutive thermal shifts, each lasting 12 s (4 s of temperature increase, 4 s of plateau, and 4 s of temperature decrease).

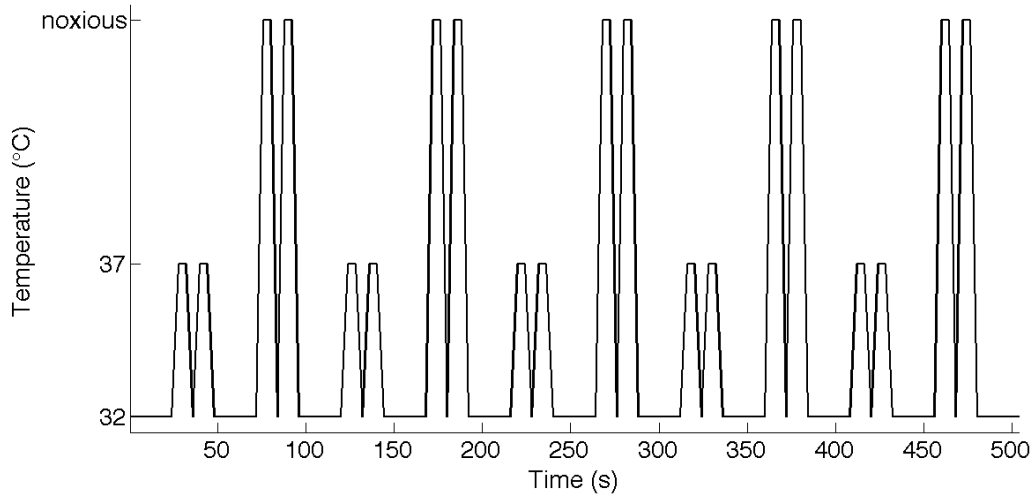

Figure 6. The graph illustrates idealized representation of the thermode's temperature during the experiment. Five non-noxious and noxious double-blocks were presented in alternating sequence. The 24-second-long double-blocks were separated by an interval of 24 seconds.

The subjects were instructed to keep their eyes closed during the experiment. The heat stimulator was observed to be sensitive to its orientation and movements within the static magnetic field. Thus, the subjects were additionally instructed not to move their legs or feet in order to keep the device stably running during the whole experiment.

4.2.2 Vicarious pain

The primary experimental stimuli consisted of a total of 120 single-foot color pictures (53 left, 67 right; normalized to 512 x 512 pixels) in painless and painful situations, as illustrated in Figure 7. Luminance was normalized across the two picture categories. The images were collected from various Internet databases. MRI-compatible goggles and response device were used to present the images to the subjects and to record their responses, respectively.

Figure 7. Vicarious pain was aroused using pictures of feet in painless and painful situations.

The experimental design followed the precedence set by Corradi-Dell'Acqua and colleagues (2011). In each trial, the pictures were presented in randomized order along with 30 null-events that consisted of a fixation cross on a black screen. The stimuli were shown for 2500 ms, and the inter-stimulus interval was randomly chosen from the set $\{2500, 2820, 3140, 3460, 3780, 4100\}$ ms. The presentation of the experimental stimuli is schematically visualized in Figure 8. The experiment lasted approximately 15 minutes.

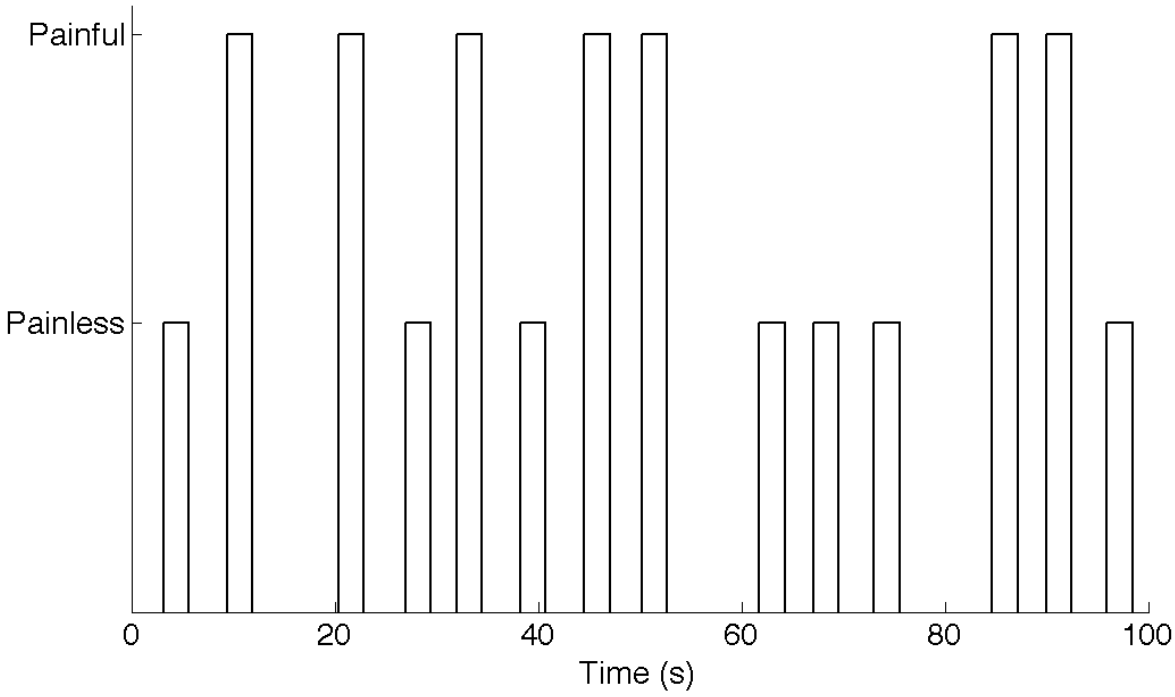

Figure 8. The graph illustrates how the pictures were presented to subjects. Only the first 100 seconds of the whole study (approx. 15 minutes) are shown.

The subjects were instructed to identify whether the presented image depicted a right or a left foot, and to signal their identification by pressing the corresponding button with the corresponding hand. The subjects were asked to respond as quickly as possible and to ignore all irrelevant features such as wounds that are shown in the pictures. Thus, no explicit demand for processing painful information was given.

After the scanning session, the subjects were asked to rate the images in four dimensions: familiarity, pain intensity, valence, and emotional intensity. The same questions and Likert-scales that were used in the study conducted by Corradi Dell'Acqua and colleagues (2011) were used in the rating task.

4.3 Imaging acquisition and preprocessing

4.3.1 Data acquisition

The measurements were conducted at the PET Centre (Turku, Finland) using a 3-Tesla MR scanner (Philips Achieva TX, Cleveland, OH). Data were acquired for both T1-weighted anatomical images and T2*-weighted MRI images with BOLD contrast. Both experiments used a repetition time of 2600 ms, an echo time of 30 ms, a flip angle of 75°, an in-plane resolution of 80 x 80 voxels (voxel size 3 mm x 3 mm), 45 slices, a slice thickness of 3 mm, and no gaps between the slices.

4.3.2 Pre-processing

A two-stage realignment procedure, i.e. a sequence of rigid-body transformations, was applied to the EPI images to correct for head movements. First, the images were realigned to the first image. Then, they were re-realigned to the mean realigned image. After the realignment procedure, the echo-planar and structural images were co-registered and normalized to the T1 standard template in MNI (Montreal Neurological Institute) space. This was done by maximizing the normalized mutual information between the images (Collignon et al. 1995). Finally, the functional images were smoothed with a three-dimensional Gaussian kernel of 8 mm full width at half maximum.

4.3.3 Data analysis

The analysis was performed using the GLM framework implemented in SPM8 (http://www.fil.ion.ucl.ac.uk/spm/) running on MATLAB 2014b.

First-level analysis

In the sensory pain experiment, the regressors of interest were created based on the stimulus functions shown in Figure 9. Three different models for the noxious and non-noxious stimuli were used, while the rest blocks were defined equally for all models.

The first model modeled the stimuli according to

$$S_i(t) = \begin{cases} 1, \text{when } \Theta(t) = \Theta_i \\ 0, \text{otherwise} \end{cases}, i = 1,2,3, \quad (9)$$

where Θ_1, Θ_2 and Θ_3 are the noxious, non-noxious and rest temperature, respectively. This choice maximally utilizes the physiological differences between perceiving pain and warmth, and it was thus expected to maximize the contrasts between the different conditions.

However, because the temperature gradients are not explicitly modeled, it is possible that the error term variances increase, weakening statistical inference. This first model is called the *event-like model* in this Thesis due to its short block-length.

In the second model, each double-block in the model is modeled using a single boxcar function, whose onset coincides with the beginning of the temperature gradient. The boxcar function was defined to be 1 for the duration of the whole block (24 s). This selection uses maximal amount of data from the measurements, and is accordingly called the *model with long blocks*. An important aspect of the model is that it assumes painful sensations also during all the temperature gradients. For example, also the expectation of pain is assumed to activate the neural circuits representing pain. If expectation activates other circuits, the signal-to-noise ratio is significantly decreased compared to the event-like model.

The third model was a compromise between these two extremes. In the *intermediate* model, each double-block was again modeled using a single boxcar function, as in the model with long blocks. However, unlike in the long blocks model, the onsets of the stimuli were defined to coincide with the beginning of the target temperature, similarly to the event-like model. The difference is that the event-like model used two short blocks for each double-block stimuli, whereas the intermediate model uses only a single block. The block was defined to last until the end of the second block's target temperature. Thus, the model assumes that the brain circuits reflecting pain are activated also during the temperature gradients between the two noxious stimulus blocks.

The stimuli in the vicarious pain experiment were modeled using delta functions corresponding to the onset times of the pictures. This way, the differences between the evoked responses elicited by the two stimulus-categories were assumed to contain minimal contribution from the handedness task, while preserving the immediate brain responses automatically caused by the onset of the stimulus.

Each regressor was convolved with the canonical HRF. The motion-related contributions to the signal were modeled using six nuisance regressors (three for translations and three for rotations, given in millimeters and radians, respectively). In addition, the mean of the signal was modeled using a constant vector. Low-frequency drifts in the signal were filtered using a cutoff period of 128 s.

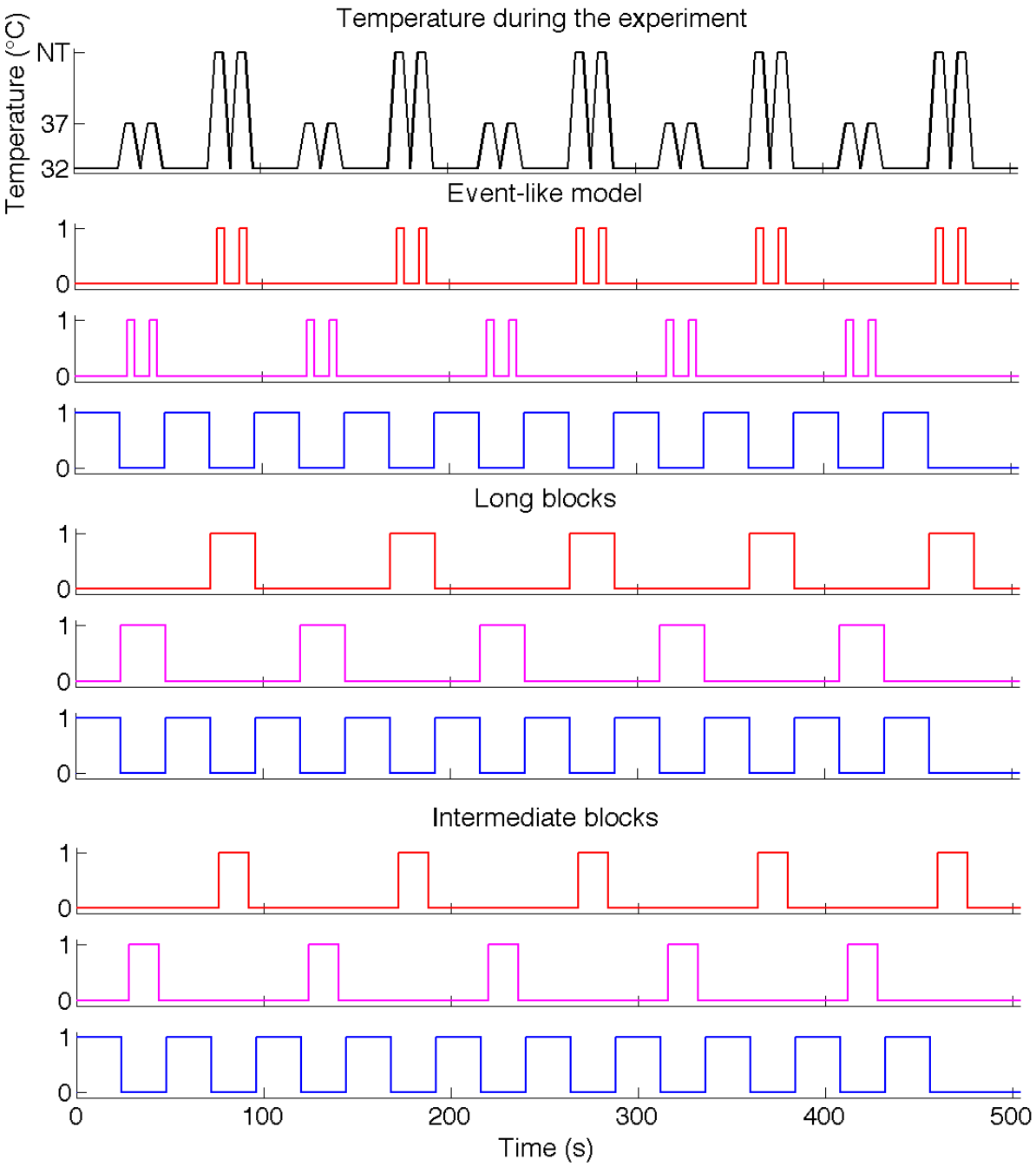

Figure 9. Illustration of the used sensory pain stimulus functions (red: noxious, magenta: non-noxious, blue: rest). NT = noxious temperature.

Second-level analysis

The first-level *t*-maps were fed into the second level analysis that used one-sample *t*-tests for each voxel to test the statistical significance of estimation across all subjects. In both experiments, random-effects analyses were used. This allows for inference about the population that the subjects represent. A significance threshold of $p < 0.01$ was used identify the activated single voxels. False discovery rate (FDR) correction was applied to reduce the number of false positive findings. All clusters with FDR-corrected $p < 0.05$ are reported.

5 Results

5.1 Sensory pain

5.1.1 Event-like model

The statistically significant clusters for the sensory pain contrast 'noxious > non-noxious' that were found by the event-like model are summarized in Table 1. Both MCC and insula exhibited bilateral neural activity increase. The MCC cluster extended through the SMA to higher motor areas, as Figure 10A shows. The ipsilateral insular activity was spread to the striatum. Also the contralateral somatosensory area corresponding to right foot showed increased activity. Ipsilaterally, increased BOLD signal was observed in hippocampus, precuneus and parietal regions. The peak T-values of the clusters ranged from 7 to 28.79.

Table 1. Clusters showing increased activity for processing noxious compared to non-noxious heat (event-like model). Shown are all FDR-corrected statistically significant clusters with a single-voxel p < 0.01. * Denotes a subcluster, located at least 8 mm from the cluster peak.

		Cluster peak MNI coordinates			Cluster	Peak
Region	Side	X	Y	Z	size	T-value
MCC	R	2	-8	46	2728	28.42
MCC	L	-6	-8	42	2728*	23.72
Insula	R	36	4	-14	815	18.31
Hippocampus	R	24	-12	-16	815*	17.57
Precuneus	R	10	-48	72	503	9.72
Postcentral gyrus	R	16	-40	72	503*	7.95
Parietal Sup	R	18	-52	68	503*	6.24
Insula	L	-36	10	12	765	8.12
Putamen	L	-28	4	10	765*	7.25
Pallidum	L	-18	6	-4	765*	7

More extensive visualization of the activation pattern can be found in Appendix A. No statistically significant *deactivation* (noxious < non-noxious) clusters were found.

5.1.2 Long block model

Three distinct clusters were identified using the model with long blocks, as shown in Table 2. As with the event-like model, both MCC and insula showed bilaterally significant increase in BOLD signal. The clusters are smaller than with the event-like model. The peak values for the clusters were 15.57, 15.5 and 8.05. The model did not reveal significant activity increase in the somatosensory areas.

Table 2. Clusters showing increased activity for processing noxious compared to non-noxious heat (long blocks model). Shown are all FDR-corrected statistically significant clusters (single-voxel p < 0.01). * Denotes a subcluster, located at least 8 mm from the cluster peak.

		Cluster peak MNI coordinates			Cluster	Peak
Region	Side	X	Y	Z	size	T-value
SMA	L	-12	2	56	1078	15.57
MCC	R	4	-4	42	1078*	14.03
MCC	L	-8	0	36	1078*	9.86
Insula	R	32	6	-6	658	15.5
Temporal Pole Sup	R	38	26	-24	658*	7.52
Frontal Inf Oper	R	62	14	4	658*	7.04
Insula	L	-36	8	-4	999	8.05
Frontal Inf Orb	L	-28	36	-6	999*	7.78

A T-map showing both statistically significant clusters is shown in Figure 10B. The pictures reveal that the cingulate cortex activity is not as obvious as it is with the event-like model. Rather, the activity is localized more to SMA. In addition, the clusters in insula significantly spread also to striatum on both hemispheres (see Appendix D for more extensive visualization of the results).

No statistically significant *deactivation* (noxious < non-noxious) clusters were found.

5.1.3 Intermediate model

The intermediate model found no statistically significant pain-induced activation or deactivation clusters.

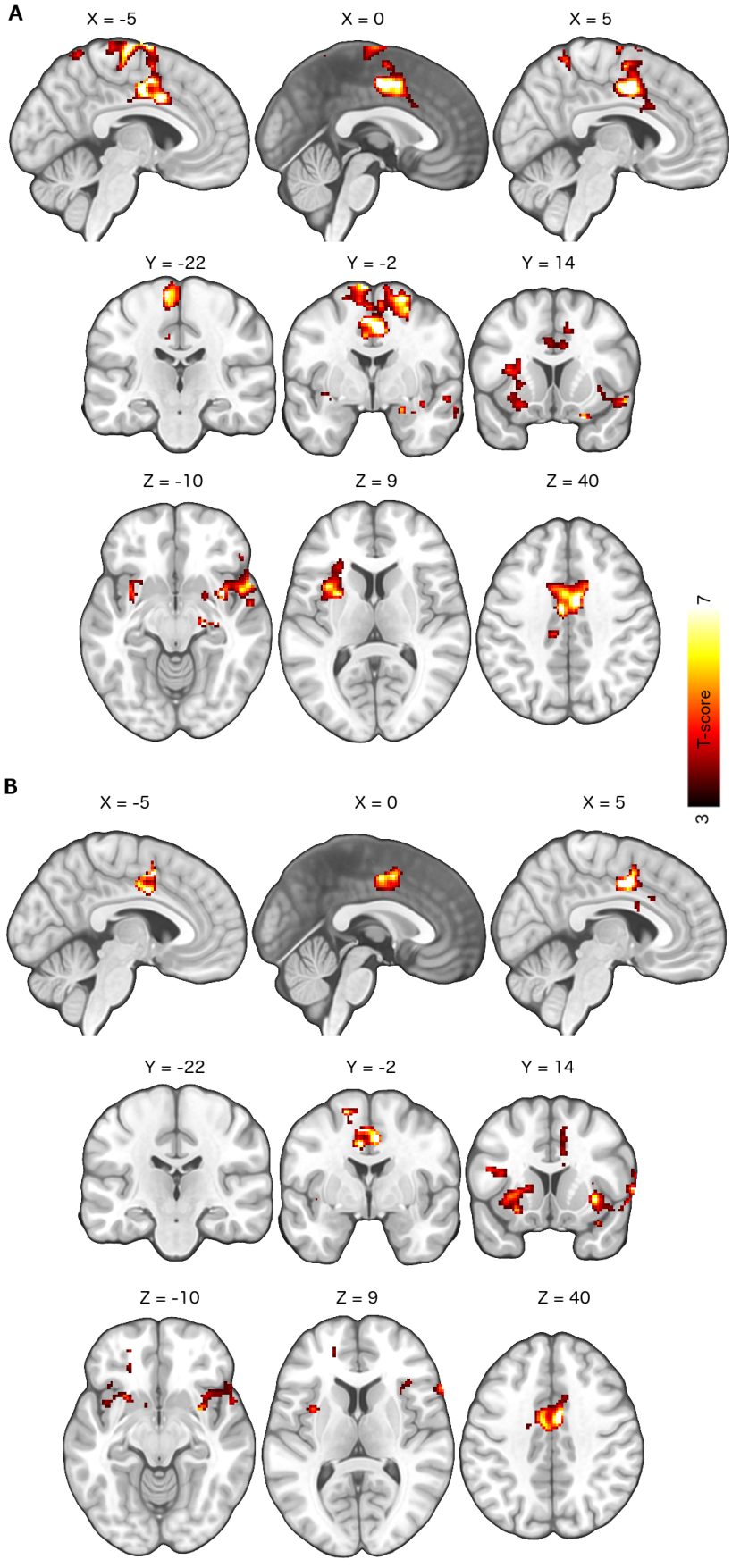

Figure 10. Sensory pain activation patterns. A: Event-like model, B: Long blocks. Statistically significant clusters (FDR-corrected $p < 0.05$, single-voxel $p < 0.01$) for contrast noxious > non-noxious are shown.

5.2 Vicarious pain

Observing painful compared to painless pictures triggered significantly increased neural activation in the brain regions reported in Table 3. Three clusters were found. The largest and most significant cluster extended bilaterally in the posterior occipital areas, the difference peak being located at right cuneus. The two other clusters located at the right posterior parietal gyrus and at a large cluster extending from the MCC to SMA. No significantly increased activity was found from somatosensory areas corresponding to right foot or from the insular cortex. The anterior insula exhibited BOLD-signal increase in response to painful pictures, but the increase did not exceed the selected significance threshold (FDR-corrected p = 0.14 for right; p = 0.24 for left hemisphere).

Table 3. Clusters showing higher activity for processing painful compared to painless pictures. Shown are all FDR-corrected statistically significant clusters with a single-voxel p < 0.01. * Denotes a subcluster, located at least 8 mm from the cluster peak.

		Cluster peak MNI coordinates			Cluster	Peak
Region	Side	X	Y	Z	size	T-value
Cuneus	R	18	-96	8	7166	30.38
Calcarine	L	-2	-88	-14	7166*	19.6
Cerebelum Crus 1	R	26	-84	-18	7166*	17.73
Parietal Inf	R	42	-42	48	395	10.2
Parietal Sup	R	26	-54	70	395*	9.76
Frontal Sup	R	16	10	48	942	9.06
MCC	L	-10	6	44	942*	7.81
SMA	R	8	10	58	942*	7.2

Figure 11 visualizes voxel wise T-values from the second level analysis superimposed on an anatomical template, showing the increased bilateral activity in the occipital areas (sagittal and axial views), in the parietal gyrus (coronal view) as well as in the MCC/SMA region (sagittal view). Of these, the MCC and SMA have been commonly reported to show increased activity for vicarious pain (Corradi-Dell'Acqua et al. 2011).

More extensive visualization of the activation pattern can be found in Appendix C. No statistically significant *deactivation* (noxious < non-noxious) clusters were found.

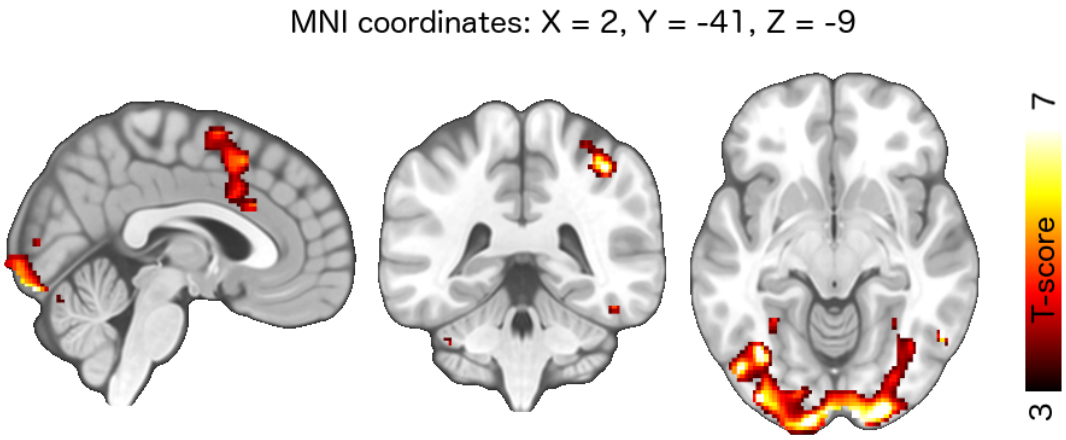

Figure 11. Vicarious pain activation pattern. Statistically significant clusters (FDR-corrected $p < 0.05$, single-voxel $p < 0.01$) for contrast painful > painless are shown.

5.3 Overlap

Both the event-like model and the model with long blocks revealed neighboring and partly overlapping neural populations in MCC/SMA for sensory and vicarious pain. The sensory pain cluster is located slightly posterior and inferior to the cluster corresponding to observing pain in others, as shown in Figure 12A (event-like model) and Figure 12B (long blocks). More extensive visualization of the overlapping activation patterns can be found in Appendices D and E.

5.4 Behavioral

The results of the behavioral task are summarized in Table 4. The participants were more familiar with the painless pictures. The painful pictures were considered to arouse more intense and negative emotions. In addition, both accuracy and reaction times were worse for the painful pictures, suggesting that their aversive nature distracted the subjects.

Table 4. Behavioral results. The values inside the parentheses represent sample standard deviations. Data from four subjects.

	Pain	Painless
Familiarity	3.79 (2.12)	6.52 (2.33)
Pain intensity	6.77 (2.78)	1.43 (0.99)
Valence	-2.91 (1.08)	-0.19 (1.08)
Emotional intensity	5.60 (2.37)	2.07 (1.33)
Accuracy	0.81 (0.13)	0.93 (0.08)
Reaction times (s)	1.34 (0.37)	1.16 (0.35)

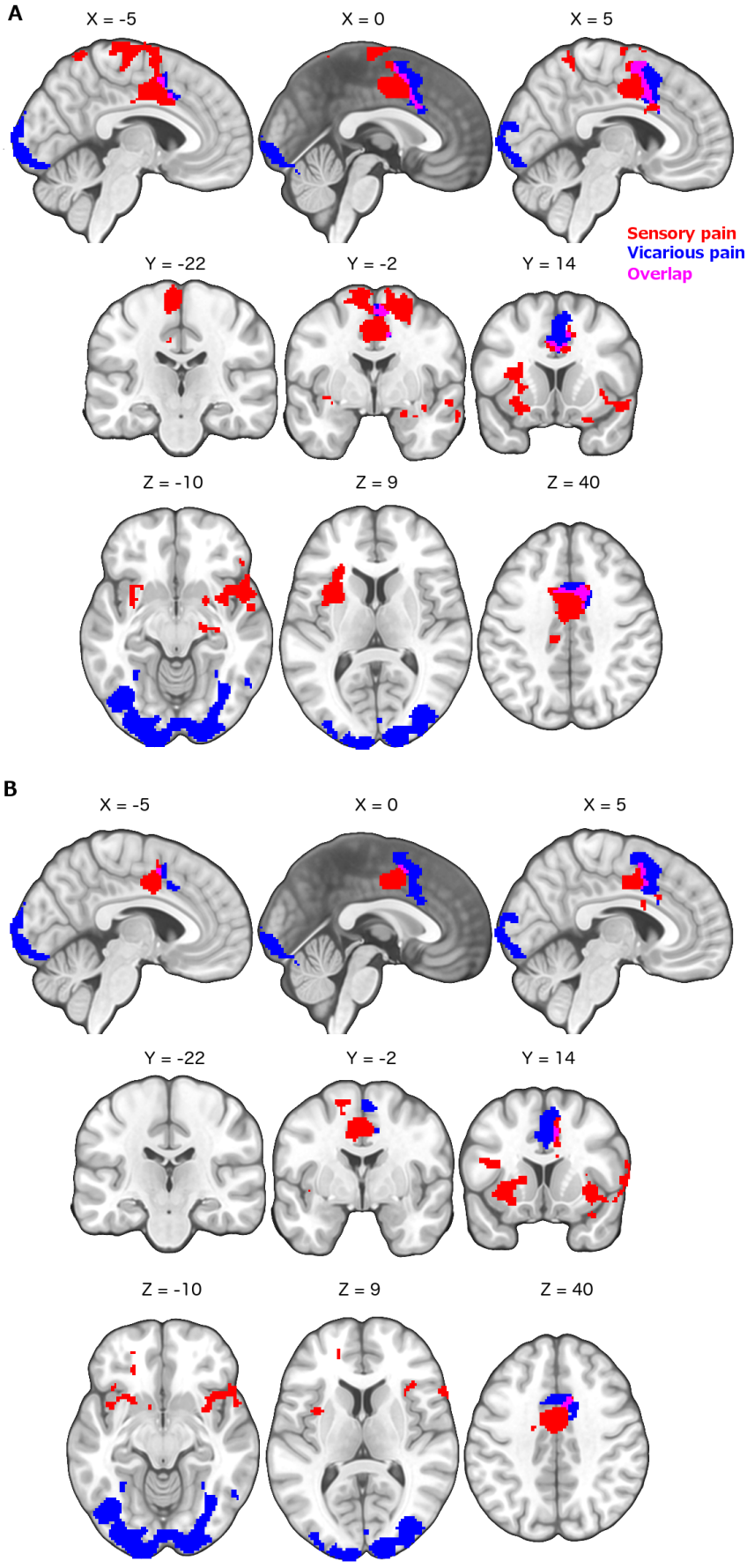

Figure 12. Sensory and vicarious pain. A = Event-like model, B = Long blocks. Shown are statistically significant (FDR-corrected, single-voxel $p < 0.01$) clusters corresponding to sensory (red) and vicarious (blue) pain (overlapping regions are shown in magenta).

6 Discussion

The Thesis provides further evidence for neighboring and slightly overlapping neural populations representing sensory and vicarious pain in an area extending from midcingulate cortex to supplementary motor area. This region exhibited statistically significant BOLD-signal increase in response to i) noxious compared to non-noxious heat, and to ii) painful compared to painless pictures. The sensory pain result was obtained using both the event-like model and the model with long blocks, suggesting that the observed activity is rather robust and potentially reflects also expectation of pain. Overall, the event-like model yielded results that most closely resemble previously reported findings on pain's neural substrates.

6.1 Help-promotion – an explanation for the observed overlap?

Both vicarious and sensory pain activated brain circuits in an area extending from the posterior midcingulate cortex to the supplementary motor area. The modality-specific circuits overlap only partially, with the sensory-pain areas represented systematically posterior to the areas representing vicarious pain. The results suggest that shared neural populations for the two stimulus-modalities do exist, but the extent of overlap is quite small.

Midcingulate cortex activity is known to reflect the aversiveness of pain perception (Foltz & White 1962), while the SMA activity represents motor preparation. Aversiveness and motor preparation are two primary components of promoting *help*. For the sufferer, the unpleasant feeling promotes pain-signaling behavior such as appropriate vocalizations and body postures. This behavior, then, enables the observer to recognize the sufferer's situation, and the automatically triggered unpleasantness promotes helping behavior (Hein et al. 2010). The motor preparation, on the other hand, prepares the sufferer to execute the pain-signaling behavior, while the observer needs the motor preparation to necessitate helping the sufferer. Thus, the cingulate cortex and supplementary motor area activity closely tie the sufferer and observer together. This theory is illustrated in Figure 13.

The anatomical proximity of the MCC and the SMA increases the credibility of the theory. Most importantly, it enables the possibility of a shared neurochemical pathway executing tasks related to both pain and empathy for pain. This would be a simple neurochemical mechanism that natural selection could have driven into existence. The endogenous opioid system is an ideal candidate for the task, as it is known to modulate sociality in animals (Machin & Dunbar 2011).

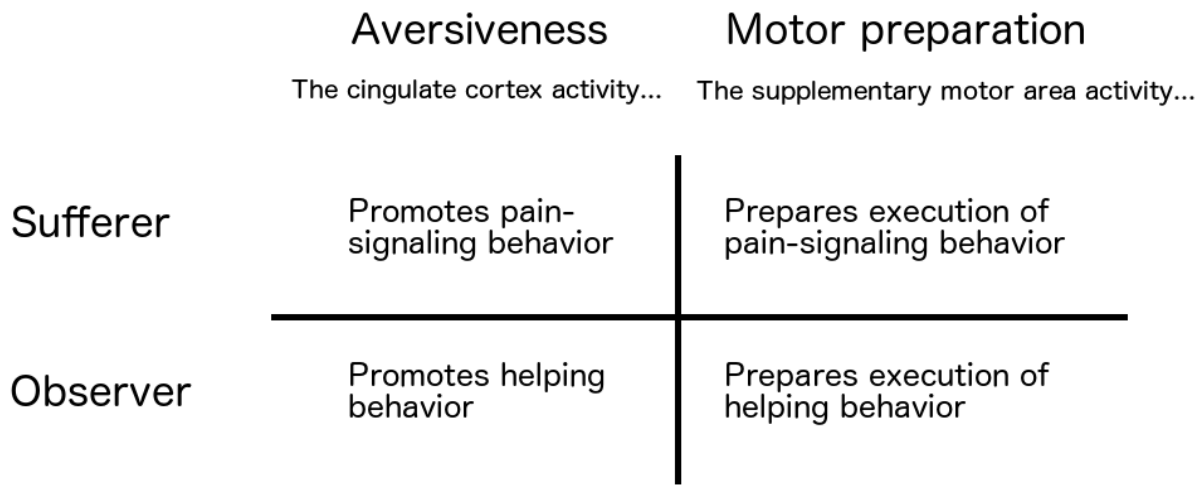

Figure 13. The matrix illustrates how help-promotion connects the shared representations for pain and empathy for pain.

The rostrocaudal neural organization of pain related to self and others, discovered by Jackson and colleagues (2006) after reviewing numerous studies on the topic, was also observed in this Thesis. It is possible that the extent of overlap between neural substrates of pain and empathy for pain has decreased over time. Perhaps the ability to understand others' painful situation originally arouse by exact replication of their affective state. The extent of overlap has since then decreased because such simulation accuracy is not needed for understanding the other. Rather, exact replication of other's affective pain sensation does not optimally serve the observer's fitness. For the observer, being able to understand but to separate the distress of oneself and the other has high evolutionary survival value. The overlap that is observed today could reflect this shift. Importantly, the shift could be executed with relatively minor changes in the gene expressions of the neighboring neuron populations.

As in most previous studies, empathy for pain did not trigger increased activity in the somatosensory cortex representing feet. This suggests that automatically recognizing the unpleasantness in the sufferer, in addition with the appropriate motor preparation, has more evolutionary value than recognizing the other's site of pain. The helping theory can explain also this phenomenon: The location of the injury does not matter in initiating helping. Rather, it is more important to understand that the other needs help and to prepare for action.

The spatial resolution of fMRI does not allow concluding whether some individual neurons were activated in response to both pain and empathy for pain. Having said that, the SMA – the superior part of the overlapping region – is among the areas where mirror neurons exist (Mukamel et al., 2010). Thus, it is possible that also the mirror neuron system contributed to the observed overlap.

6.2 Comparison of the sensory pain models

6.2.1 Event-like model

The event-like model of pain perception yielded results that closely match previously reported findings on brain representations of sensory pain: Increased activity was observed bilaterally in MCC/SMA and insula, contralaterally in the somatosensory cortex region that represents the stimulated foot and Ipsilaterally in hippocampus. All of these areas have been previously reported to be associated with sensory pain (Peyron et al. 2000; Corradi-Dell'Acqua et al. 2011; Wager et al. 2013; Tracey & Mantyh 2007). In addition, ipsilateral precuneus exhibited statistically significant activity increase. Previous reports on the region's role in pain perception is contradictory: BOLD signal from precuneus has been previously reported to be both increased (Lamm et al. 2011) and decreased (Corradi-Dell'Acqua et al. 2011; Wager et al. 2013) in response to noxious compared to non-noxious stimulus. The area's role in pain perception remains mysterious.

Among the tested models, the event-like model yielded results that best accord with existing literature on brain's pain-circuits. Considering the pain-specificity of nociceptors that was discussed in Chapter 2.1.1, this comes as no surprise, as the event-like model defines pain perception very conservatively: Because nociceptors do not activate until the temperature increases above subject's pain threshold, and because the noxious temperature was defined to equal the pain threshold of each subject, it makes sense that the model predicts the hemodynamic response to painful stimulus better than any of the two other stimuli.

Unlike the two other models, the event-like model left the temperature gradients to be completely modeled by the motion regressors. The results suggest that it did not matter. However, it is possible that including one or two nuisance regressors for the temperature gradients could further improve the model. A simple possibility would be to model both the up-and-downward gradients with a delta function at the onset of the gradient. Another option would be to use one regressor for increasing and another for decreasing temperature gradient. Increasing the number of regressors would likely lead to better fit to data, but that would come with a cost of decreased number of freedom. Experiments would have to be done to see whether the increased accuracy would be worth the increased complexity of the model.

6.2.2 Long blocks model

Also the model with long blocks yielded results that are in good agreement with previous findings. The MCC/SMA and insula were activated bilaterally. However, unlike the event-

like model, the long blocks model found no significant differences between noxious and non-noxious heat in somatosensory cortex areas representing the stimulated foot. As the model implicitly assumed that expectation of pain activates same brain regions that experiencing pain does, it seems that the somatosensory region, unlike the affective components of the pain matrix, was not activated by expectation of pain.

The peak T-values of the clusters are systematically and significantly lower compared to those obtained by the event-like model. This is another indicator of the event-like model's superiority on distinguishing between noxious and non-noxious heat. Because of its poorer fit and the interpretation problems, the long blocks model does not seem to have any advantages compared to the event-like model.

6.2.3 Intermediate blocks model

The intermediate model found no statistically significant clusters. This is surprising as the two extreme models found differences between the two conditions at expected locations.

If the event-like model were the only model showing reasonable activity pattern, it would be easy to dismiss the two other models based on their poorer signal-to-noise ratio. However, also the long blocks model captured the affective components of sensory pain, even though it should have the lowest signal-to-noise ratio among the models. On the other hand, if the long blocks model worked and the event-like model did not, the logical conclusion would be that the pain perception onsets for the event-like model were incorrectly modeled, that in reality, the perception begins earlier and perhaps lasts longer than was supposed. Neither of these hypothetical situations applies here.

The only logical conclusion that can be made based on the results, it seems, is that the temperature gradients *between* the double-blocks somehow distort the results, but that the outermost gradients do not. When the in-between gradients are excluded, as in the event-like model, the results are in-line with previous findings. When they are included, but constitute only a quarter of the block-length, as in the model with long blocks, their effect is sufficiently weak not to dramatically distort the results. However, when they constitute fifty percentage of the block-length, as in the intermediate block-length model, the signal-to-noise ratio significantly decreases and the pain-associated brain activity pattern disappears.

What could be underlying such strange phenomenon? Because no significantly increased neural activation was identified in the whole brain, it seems that there is significant variation in the brain activity during the in-between temperature gradients. A simple explanation would

be that the inter-subject variation during the transition period was extremely high. Given the low number of participants, it is impossible to exclude that option. In addition, also within-subject variability could have contributed to the variation. Within-subject variation could arise from, for example, subjects being slightly anxious about the shortly coming noxious temperature at the beginning of the experiment, while being more comfortable later due to physiological and psychological habituation to the stimulus. Whatever the reason, the results suggest that the intermediate model does not capture the pain-associated brain activity at all, and the model should not be used in experiments that investigate brain's pain processing.

6.2.4 Deactivation patterns

No statistically significant deactivation clusters were found. The lack of deactivation clusters suggests either that i) pain really induced little deactivation in the brain or ii) deactivation is less intense than activation in response to pain. In addition, it is possible that both are true. Without further experiments, it is impossible to abandon neither option. However, the second option does seem logical. Given the biological role of pain as a warning signal of potential tissue damage, the signal needs to be strong to induce an easily detectable contrast to a baseline. In addition, because the default activity of neurons is relatively low, the only possibility to signal such potent information to the perceiver is to increase, not decrease the intensity of firing. To simplify, dropping activity from zero is impossible, while high activity increases are possible. This might also explain the low number of existing reports of pain-induced deactivation patterns.

6.3 Vicarious pain

Clusters exhibiting increased BOLD-signal in response to painful compared to painless pictures were found in occipital cortex, right posterior parietal gyrus and bilateral MCC/SMA. The results accord with existing literature (Zubieta et al. 2001; Jackson et al. 2006; Corradi-Dell'Acqua et al. 2011; Wager et al. 2013), although the author is not aware of any single study identifying all three areas simultaneously representing vicarious pain.

Increased occipital activity has been previously reported to also reflect processing disgusting visual stimuli (Schienle et al. 2006) and attention tasks (Chung et al. 2014). This is worth noting for two reasons. First, some subjects in this study reported afterwards that the used pictures were disgusting as much as painful, so whether the evoked activation really represents disgust or pain remains unknown. In addition, many subjects said that the handedness task was much more difficult for the painful pictures. Both the response times and

accuracy percentages of the handedness task were worse for painful pictures, suggesting that the handedness task really demanded more attention during the painful pictures. Thus, it is possible that the attention processes also contributed to the increased occipital activity. This does not seem as likely explanation as the disgust, however, because the picture stimuli were modeled using delta functions that should poorly predict long-lasting psychological processes such as attention. To conclude, it seems likely that the observed occipital activity increase was caused by automatic emotional (pain or disgust) processes rather than long-lasting attention processes. To distinguish between pain and disgust, a new stimulus set with less disgusting features should be created.

Anterior insula at both hemispheres exhibited increased, but not significantly increased, activity for painful compared to painless pictures ($p < 0.15$ for right, $p < 0.24$ for left hemisphere). Despite statistical insignificance, the result deserves to be mentioned because previous studies have systematically associated increased BOLD-signal in bilateral anterior insula with vicarious pain. It seems that the used stimulus set did activate the insula also in this study, but across-subject variation – which can be rather high with such few participants, even if an effect exists – caused the lack of significance.

6.4 Conclusions

The aim of the study was to investigate brain circuits of sensory and vicarious pain, induced by noxious heat and pictures of feet in pain. As in many previous studies, both sensory and vicarious pain triggered robust activity increase in partly overlapping but mostly neighboring neural populations in an area extending bilaterally from midcingulate cortex to supplementary motor area. The self-related pain circuits were located slightly posterior to the other-related circuits. Modality-specific brain regions exhibiting increased activation to the corresponding stimulus included somatosensory cortex and bilateral insula for sensory pain and occipital cortex for vicarious pain. Evolutionary benefits of promoting helping behavior were suggested to account for the observed similarities between the neural representations of the two stimulus modalities. As the only model identifying the primary somatosensory cortex as a part of the brain's pain network, the event-like model yielded results that best accord with existing literature. Because also the model's interpretation is straightforward compared to the other models, its use is highly encouraged in future studies investigating the neural basis of sensory pain.

Bibliography

Apkarian AV, Bushnell MC, Treede RD, Zubieta JK. Human brain mechanisms of pain perception and regulation in health and disease. *European Journal of Pain*. 2005, 9(4), pp. 463–484.

Attwell, D, Buchan AM, Charpak S, Lauritzen M, Macvicar, BA, Newman, EA. Glial and neuronal control of brain blood flow. *Nature*. 2010, 468(7321), pp. 232–43.

Avenanti AV, Bueti D, Galati G, Aglioti SM. Transcranial magnetic stimulation highlights the sensorimotor side of empathy for pain. *Nature Neuroscience*. 2005, 8(7), pp. 955–960.

Baliki MN, Chialvo DR, Geha PY, Levy RM, Harden RN, Parrish TB, AV Apkarian. Chronic pain and the emotional brain: specific brain activity associated with spontaneous fluctuations of intensity of chronic back pain. *The Journal of Neuroscience.* 2006, 26(47), pp. 12165–12173.

Basbaum AI, Fields HL. Endogenous pain control systems: brainstem spinal pathways and endorphin circuitry. *Annual Review of Neuroscience*. 1982, 7, pp. 309–338.

Behbehani MM. Functional characteristics of the midbrain periaqueductal gray. *Progress in Neurobiology*. 1995, 46, pp. 575–605.

Bennett DLH, Woods CG. Painful and painless channelopathies. *The Lancet Neurology*. 2014, 13, pp. 587–599.

Bernhardt BC, Singer T. The neural basis of empathy. *Annual Review of Neuroscience*. 2012, 35, pp. 1–23.

Besson JM. The neurobiology of pain. *Lancet.* 1999, 353(9164), pp. 1610–1615.

Bessou PP, Perl ER. Response of cutaneous sensory units with unmyelinated fibers to noxious stimuli. *Journal of Neurophysiology*. 1969, 32(6), pp. 1025–1043.

Botvinick M, Jha AP, Bylsma LM, Fabian SA, Solomon PE, Prkachin KM. Viewing facial expressions of pain engages cortical areas involved in the direct experience of pain. *Neuroimage*. 2005, 25(1), pp. 312–319.

Boynton GM, Engel SA, Glover GH, Heeger DJ. Linear systems analysis of functional magnetic resonance imaging in human V1. *The Journal of Neuroscience*. 1996, 16(13), pp. 4207–4221.

Bufalari I, Aprile T, Avenanti AV, Di Russo F, Aglioti SM. Empathy for pain and touch in the human somatosensory cortex. *Cerebral Cortex*. 2007, 17(11), pp. 2553–2561.

Carr L, Iacaboni M, Dubeau M-C, Mazziotta JC, Lenzi GL. Neural mechanisms of empathy in humans: a relay from neural systems for imitation to limbic areas. *Proceedings of the National Academy of Sciences of the United States of America*. 2003, 100(9), pp. 5497–5502.

Chavhan GB, Babyn PS, Thomas B, Shroff MM, Haacke EM. Principles, techniques, and applications of T2*-based MR imaging and its special applications. *Radiographics*. 2009, 29(5), pp. 1433–1449.

Chung S-C, Choi M-H, Kim H-S, You N-R, Hong S-P, Lee J-C, Park S-J, Baek J-H, Jeong U-H, You J-H, Lim D-W, Kim H-J. Effects of distraction task on driving: a functional magnetic resonance imaging study. *Bio-medical Materials and Engineering*. 2014, 24(6), pp. 2971–2977.

Collignon A, Maes F, Delaere D, Vandermeulen D, Suetens P, Marchal G. Automated multi-modality image registration based on information theory. *Information Processing in Medical Imaging*. 1995, 3(6), pp. 263–274.

Corradi-Dell'Acqua C, Hofstetter C, Vuilleumier P. Felt and seen pain evoke the same local patterns of cortical activity in insular and cingulate cortex. *The Journal of Neuroscience*. 2011, 31(49), pp. 17996–18006.

Darwin C. On the origin of species by means of natural selection. John Murray, London, 1859. p. 197.

Decety, J. Dissecting the Neural Mechanisms Mediating Empathy. *Emotion Review*. 2011, 3(1), pp. 92–108.

Descartes R. The world and other writings. Translated and edited by Gaukroger S. Cambridge University Press, 2004. ISBN 0-511-03579-9. pp. 117-118.

Farrell MJ, Laird AR, Egan GF. Brain activity associated with painfully hot stimuli applied to the upper limb: a meta-analysis. *Human Brain Mapping*. 2005, 25(1), pp. 129–139.

Ferrari PF, Rizzolatti G. Mirror neuron research: the past and the future. *Philosophical Transactions of the Royal Society B*. 2014, 369(1644): 20130169.

Fields H. State-dependent opioid control of pain. *Nature Reviews Neuroscience*. 2004, 5(7), pp. 565–575.

Foltz EL, White LE. Pain "relief" by frontal cingulotomy. *Journal of Neurosurgery*. 1962, 19, pp. 89–100.

Fox MD, Raichle ME. Spontaneous fluctuations in brain activity observed with functional magnetic resonance imaging. *Nature Reviews Neuroscience*. 2007, 8(9), pp. 700–711.

Friston KJ. Characterizing dynamic brain responses with fMRI: a multivariate approach. *Neuroimage*. 1995, 2, pp. 166–172.

Friston KJ, Holmes AP, Worsley KJ, Poline J-P, Frith CD, Frackowiak RSJ. Statistical parametric maps in functional imaging: a general linear approach. *Human Brain Mapping*. 1995, 2, pp. 189–210.

Friston KJ, Fletcher P, Josephs O, Holmes A, Rugg MD, Turner R. Event-related fMRI: characterizing differential responses. *Neuroimage.* 1998, 7(1), pp. 30–40.

Friston KJ, Mechelli A, Turner R, Price CJ. Nonlinear responses in fMRI: the Balloon model, Volterra kernels, and other hemodynamics. *Neuroimage*. 2000, 12(4), pp. 466–477.

Gallese V. The manifold nature of interpersonal relations: the quest for a common mechanism. *Philosophical Transactions of the Royal Society B*. 2003, 358(1431), pp. 517–528.

Gallese V, Goldman A. Mirror neurons and the simulation theory of mind-reading. *Trends in Cognitive Sciences*. 1998, 2(12), pp. 493–501.

Garland EL. Pain processing in the human nervous system: a selective review of nociceptive and biobehavioral pathways. *Primary Care*. 2012, 39(3), pp. 561–571.

Gebhart GF. Descending modulation of pain. *Neuroscience and Biobehavioral Reviews*. 2004, 27(8), pp. 729–737.

Gould SJ, Vrba ES. Exaptation-a missing term in the science of form. *Paleobiology*. 1982, 8, pp. 4–15.

Hadjipavlou G, Dunckley P, Behrens TE, Tracey I. Determining anatomical connectivities between cortical and brainstem pain processing regions in humans: a diffusion tensor imaging study in healthy controls. *Pain*. 2006, 123(1-2), pp. 169–178.

Hein G, Silani G, Preuschoff K, Batson D, Singer T. Neural responses to ingroup and outgroup members' suffering predict individual differences in costly helping. *Neuron*. 2010, 68(1), pp. 149–160.

Hillman EMC. Coupling mechanism and significance of the BOLD signal: a status report. *Annual Review of Neuroscience.* 2014, 37, pp. 161–181.

Huettel SA, Song AW, McCarthy G. Functional magnetic resonance imaging. Second edition. Sinauer Associates, Inc. Publishers Sunderland, Massachusetts U.S.A. 2009. ISBN: 978-0-87893-286-3. 512 p.

Iacoboni M. Imitation, empathy, and mirror neurons. *Annual Review of Psychology*. 2009, 60, pp. 653–670.

Jackson PL, Brunet E, Meltzoff AN, Decety J. Empathy examined through the neural mechanisms involved in imagining how I feel versus how you feel pain. *Neuropsychologia*. 2006, 44, pp. 752–761.

Jackson PL, Meltzoff AN, Decety J. How do we perceive the pain of others? A window into the neural processes involved in empathy. *Neuroimage*. 2005, 24(3), pp. 771–779.

Jackson PL, Rainville PP, Decety J. To what extent do we share the pain of others? Insight from the neural bases of pain empathy. *Pain*. 2006, 125(1-2), pp. 5–9.

Jezzard P, Clare S. Principles of nuclear magnetic resonance and MRI. In: Jezzard P, Matthew PM, Smith SM (eds). *Functional MRI: an introduction to methods*. Oxford university press, 2002, Oxford. ISBN: 019852773X. pp. 67-92.

Kiebel SJ, Holmes AP. The general linear model. In: Friston KJ, Ashburner JT (eds). *Statistical parametric mapping: the analysis of functional brain images*. Academic press. 2006. ISBN: 9780080466507. pp. 101-125.

Lamm C, Nusbaum HC, Meltzoff AN, Decety J. What are you feeling? Using functional magnetic resonance imaging to assess the modulation of sensory and affective responses during empathy for pain. *PLoS ONE*. 2007, 2(12), e1292.

Lamm C, Decety J, Singer T. Meta-analytic evidence for common and distinct neural networks associated with directly experienced pain and empathy for pain. *Neuroimage*. 2011, 54(3), pp. 2492–2502.

Lamm C, Majdandžić J. The role of shared neural activations, mirror neurons, and morality in empathy – a critical comment. *Neuroscience Research*. 2014 (in press).

Lange N, Zeger SL. Non-linear Fourier time series analysis for human brain mapping by functional magnetic resonance imaging. *Journal of the Royal Statistical Society. Series C (Applied Statistics)*. 1997, 46(1), pp. 1–29.

Legrain V, Iannetti GD, Plaghki L, Mouraux A. The pain matrix reloaded: A salience detection system for the body. *Progress in Neurobiology*. 2011, 93(1), pp. 111–124.

Logothetis NK, Pauls J, Augath M, Trinath T, Oeltermann A. Neurophysiological investigation of the basis of the fMRI signal. *Nature*. 2001, 412(6843), pp. 150–157.

Machin AJ, Dunbar RI. The brain opioid theory of social attachment: a review of the evidence. *Behaviour*. 2011, 148(9), pp. 985–1025.

Malonek D, Grinvald A. Interactions between electrical activity and cortical microcirculation revealed by imaging spectroscopy: implications for functional brain mapping. *Science*. 1996, 272, pp. 551–554.

Mansfield P. Multi-planar image formation using NMR spin echoes. *Journal of Physics C: Solid State Physics*. 1977, 10, pp. 55–58.

Mantyh PW, Peschanski M. Spinal projections from the periaqueductal grey and dorsal raphe in the rat, cat and monkey. *Neuroscience*. 1982, 7(11), pp. 2769–2776.

Melzack R. From the gate to the neuromatrix. *Pain*. 1999, 82, pp. 121–126.

Mendell LM. Constructing and deconstructing the gate theory of pain. Pain. 2014, 155(2), pp. 210–216.

Michael J, Sandberg K, Skewes J, Wolf T, Blicher J, Overgaard M, Frith CD. Continuous theta-burst stimulation demonstrates a causal role of premotor homunculus in action understanding. *Psychological Science.* 2014, 25(4), pp. 963–972.

Mitchell JP. Inferences about mental states. *Philosophical Transactions of the Royal Society B*. 2009, 364(1521), pp. 1309–1316.

Mouraux A, Diukova A, Lee MC, Wise RG, Iannetti GD. A multisensory investigation of the functional significance of the "pain matrix". *Neuroimage*. 2011, 54(3), pp. 2237–2249.

Mukamel R, Ekstrom AD, Kaplan J, Iacaboni M, Fried I. Single-neuron responses in humans during execution and observation of actions. *Current Biology*. 2010, 20(8), pp. 750–756.

Nishitani N, Hari R. Temporal dynamics of cortical representation. *Proceedings of the National Academy of Sciences of the United States of America*. 2000, 97(2), pp. 913–918.

Ogawa S, Lee TM, Kay AR, Tank DW. Brain magnetic resonance imaging with contrast dependent on blood oxygenation. *Proceedings of the National Academy of Sciences of the United States of America*. 1990, 87(24), pp. 9868–9872.

Pauling L, Coryell CD. The magnetic properties and structure of hemoglobin, oxyhemoglobin and carbonmonoxyhemoglobin. *Proceedings of the National Academy of Sciences of the United States of America*. 1936, 22(4), pp. 210–216.

Di Pellegrino G, Fadiga L, Fogassi L, Gallese V, Rizzolatti G. Understanding motor events: a neurophysiological study. *Experimental Brain Research*. 1992, 91, pp. 176–180.

Peyron R, Laurent B, García-Larrea L. Functional imaging of brain responses to pain. A review and meta-analysis. *Clinical Neurophysiology*. 2000, 30(5), pp. 263–288.

Reynolds DV. Surgery in the rat during electrical analgesia induced by focal brain stimulation. *Science*. 1969, 164, pp. 444–445.

Rizzolatti G, Craighero L. The mirror-neuron system. *Annual Review of Neuroscience*. 2004, 27, pp. 169–192.

Roy CS, Sherrington CS. On the regulation of the blood-supply of the brain. *The Journal of Physiology*. 1890, 11(1-2), pp. 85–108.

Schienle A, Schäfer A, Hermann A, Walter B, Stark R, Vaitl D. fMRI responses to pictures of mutilation and contamination. *Neuroscience Letters*. 2006, 393(2-3), pp. 174–178.

Sherrington CS. Qualitative difference of spinal reflex corresponding with qualitative difference of cutaneous stimulus. *The Journal of Physiology*. 1903, 30(1), pp. 39–46.

Singer T, Seymour B, O'Doherty J, Kaube H, Dolan RJ, Frith CD. Empathy for pain involves the affective but not sensory components of pain. *Science*. 2004, 303(5661), pp. 1157–1162.

Singer T, Lamm C. The social neuroscience of empathy. *Annals of the New York Academy of Sciences*. 2009, 1156, pp. 81–96.

Tortora G, Derrickson B. *Principles of anatomy & physiology: Organization, support, and movement, and control systems of the human body*. 13th edition. John Wiley & Sons, Inc., 2011. ISBN: 978-0-470-64608-3. pp. 450-474.

Tracey I. Getting the pain you expect: mechanisms of placebo, nocebo and reappraisal effects in humans. *Nature Medicine*. 2010, 16(11), pp. 1277–1283.

Tracey I, Mantyh PW. The cerebral signature for pain perception and its modulation. *Neuron*. 2007, 55(3), pp. 377–391.

Tölle TR, Kaufmann T, Siessmeier T, Lautenbacher S, Berthele A, Munz F, Zieglgänsberger W, Willoch F, Schwaiger M, Conrad B, Bartenstein P. Region-specific encoding of sensory and affective components of pain in the human brain: a positron emission tomography correlation analysis. *Annals of Neurology*. 1999, 45(1), pp. 40–47.

De Waal FBM. Putting the altruism back into altruism: the evolution of empathy. *Annual Review of Psychology*. 2008, 59, pp. 279–300.

Wager TD, Atlas LY, Lindquist MA, Roy M, Woo C-W, Kross E. An fMRI-based neurologic signature of physical pain. *The New England Journal of Medicine*. 2013, 368(15), pp. 1388–1397.

Wager TD, Rilling JK, Smith EE, Sokolik A, Casey KL, Davidson RJ, Kosslyn SM, Rose RM, Cohen JD. Placebo-induced changes in fMRI in the anticipation and experience of pain. *Science*. 2004, 303(5661), pp. 1162–1167.

Wey H-Y, Catana C, Hooker JM, Dougherty DD, Knudsen GM, Wang DJJ, Chonde BD, Rosen BR, Gollub RL, Kong J. Simultaneous fMRI-PET of the opioidergic pain system in human brain. *Neuroimage*. 2014, 102, 2, pp. 275–282.

Willis WD, Westlund KN. Neuroanatomy of the pain system and of the pathways that modulate pain. *Journal of Clinical Neurophysiology*. 1997, 14, pp. 2–31.

Woolf CJ, Ma Q. Nociceptors–noxious stimulus detectors. *Neuron*. 2007, 55(3), pp. 353–364.

Worsley KJ. Principles of nuclear magnetic resonance and MRI. In: Jezzard P, Matthew PM, Smith SM (eds). *Functional MRI: an introduction to methods*. Oxford university press, 2002, Oxford. ISBN: 019852773X. pp. 251-270.

Zubieta JK, Smith YR, Bueller JA, Xu Y, Kilbourn MR, Jewett DM, Meyer CR, Koeppe RA, Stohler CS. Regional mu opioid receptor regulation of sensory and affective dimensions of pain. *Science*. 2001, 293(5528), pp. 311–315.

APPENDICES

A. Visualization of the brain activation pattern representing sensory pain (event-like model).

B. Visualization of the brain activation pattern representing sensory pain (long blocks model).

C. Visualization of the brain activation pattern representing vicarious pain.

D. Visualization of the brain activation patterns of sensory and vicarious pain (event-like model).

E. Visualization of the brain activation patterns of sensory and vicarious pain (long blocks model).

Appendix A. Sensory pain, event-like model (noxious > non-noxious)

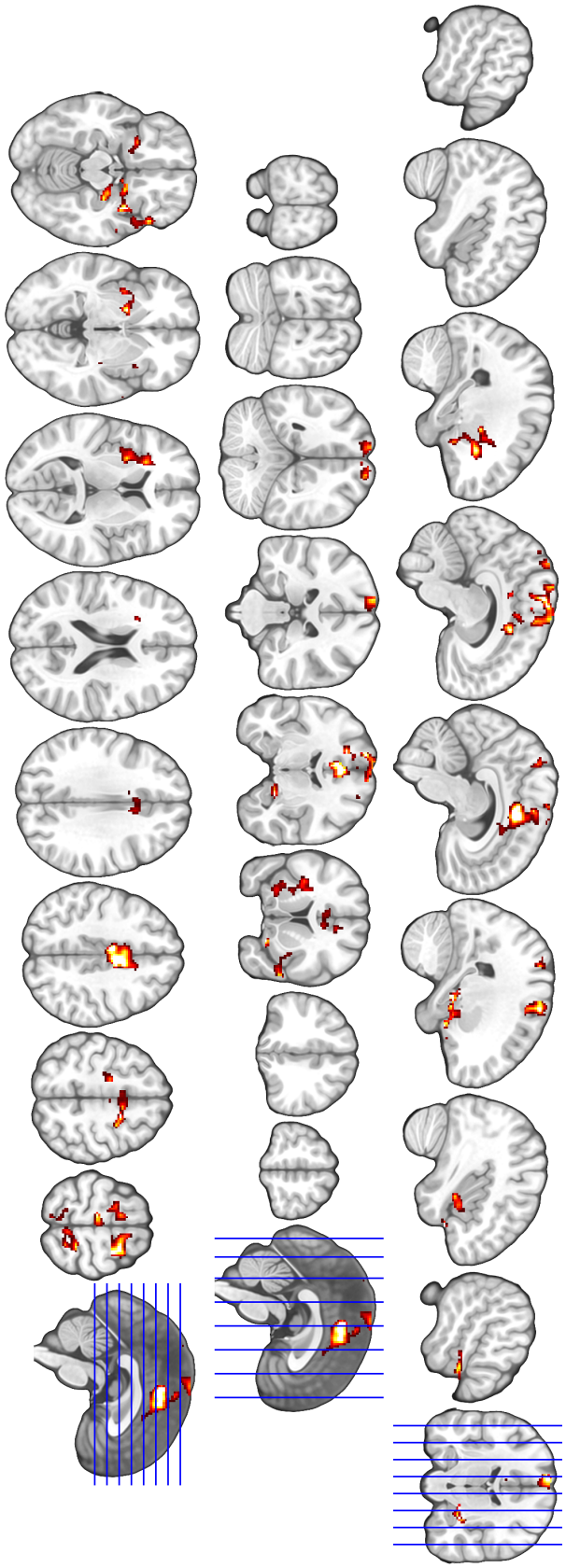

Figure 14. Visualization of the statistically significant clusters (FDR-corrected p < 0.05, single-voxel p < 0.01) for contrast noxious > non-noxious using the event-like model.

Appendix B. Sensory pain, long blocks model (noxious > non-noxious)

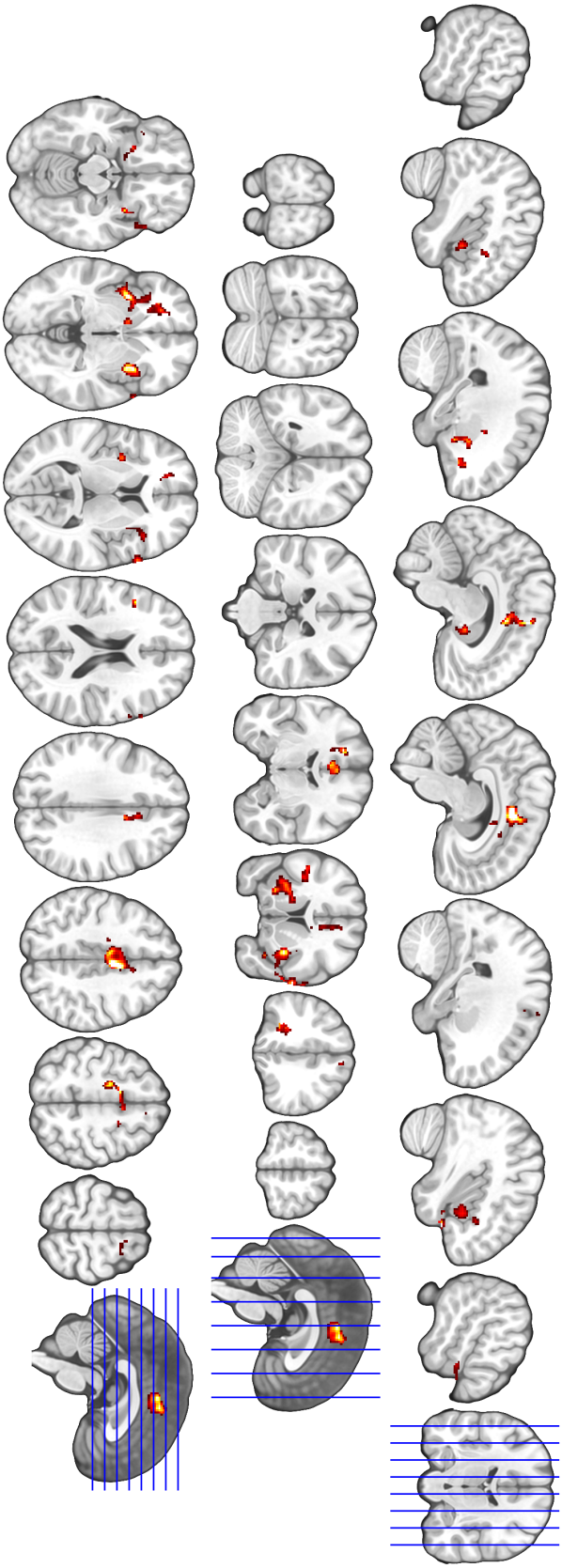

Figure 15. Visualization of the statistically significant clusters (FDR-corrected p < 0.05, single-voxel p < 0.01) for contrast noxious > non-noxious using the long blocks model.

Appendix C. Vicarious pain (painful > painless)

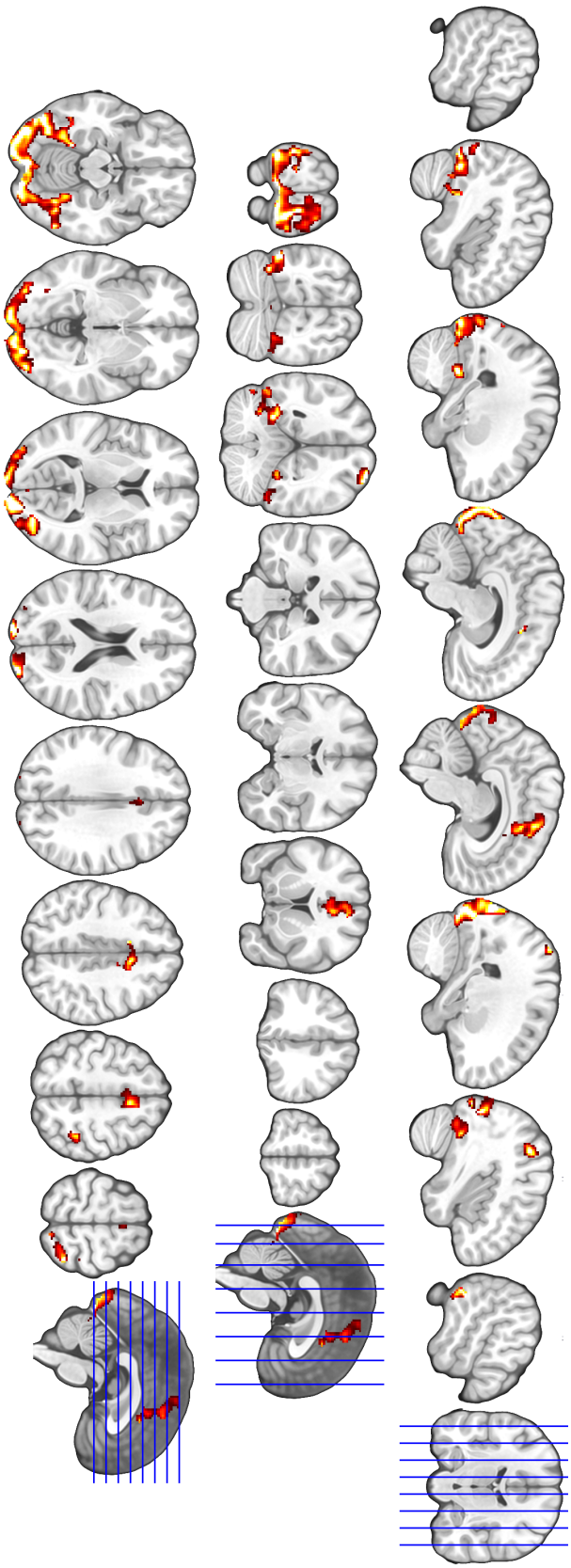

Figure 16. Visualization of the statistically significant clusters (FDR-corrected p < 0.05, single-voxel p < 0.01) for contrast painful > painless.

Appendix D. Overlap of sensory and vicarious pain (event-like model).

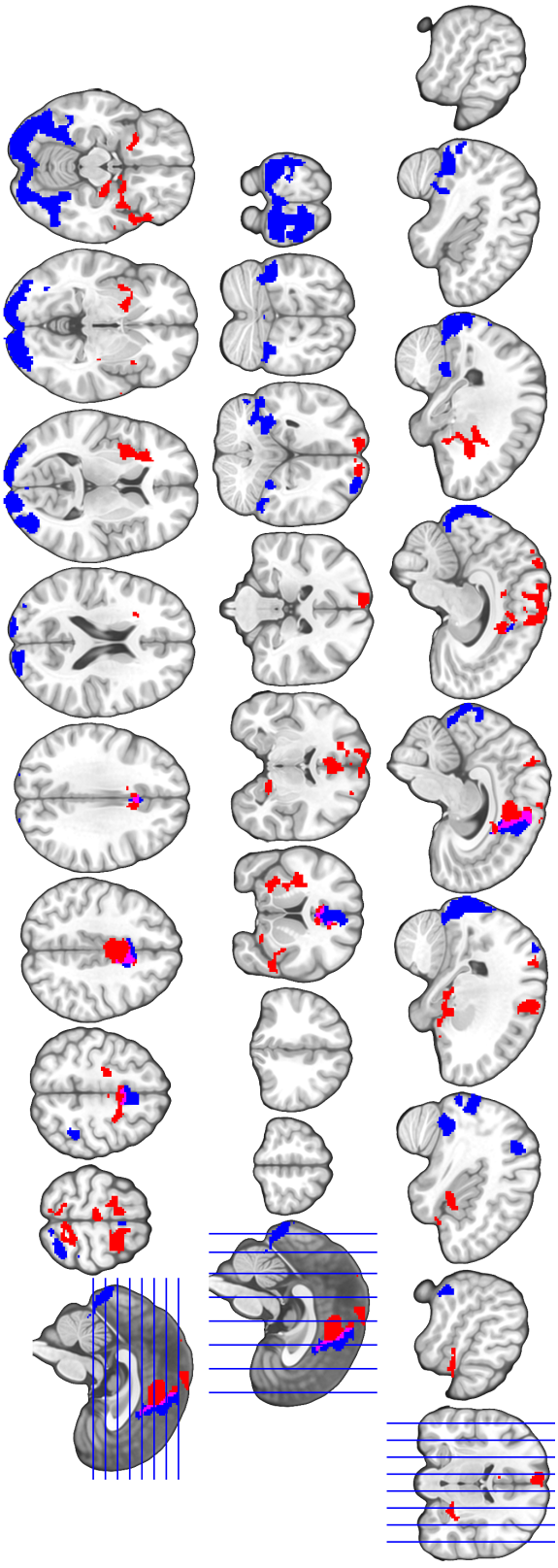

Figure 17. Comparison of the activation patterns for directly (red) and vicariously (blue) experienced pain (overlapping areas are shown in magenta). FDR-corrected ($p < 0.05$) statistically significant clusters (single-voxel $p < 0.01$) are shown for sensory pain, while FDR-corrected (single-voxel $p < 0.01$) are shown for vicarious pain.

Appendix E. Comparison of sensory and vicarious pain (long blocks model).

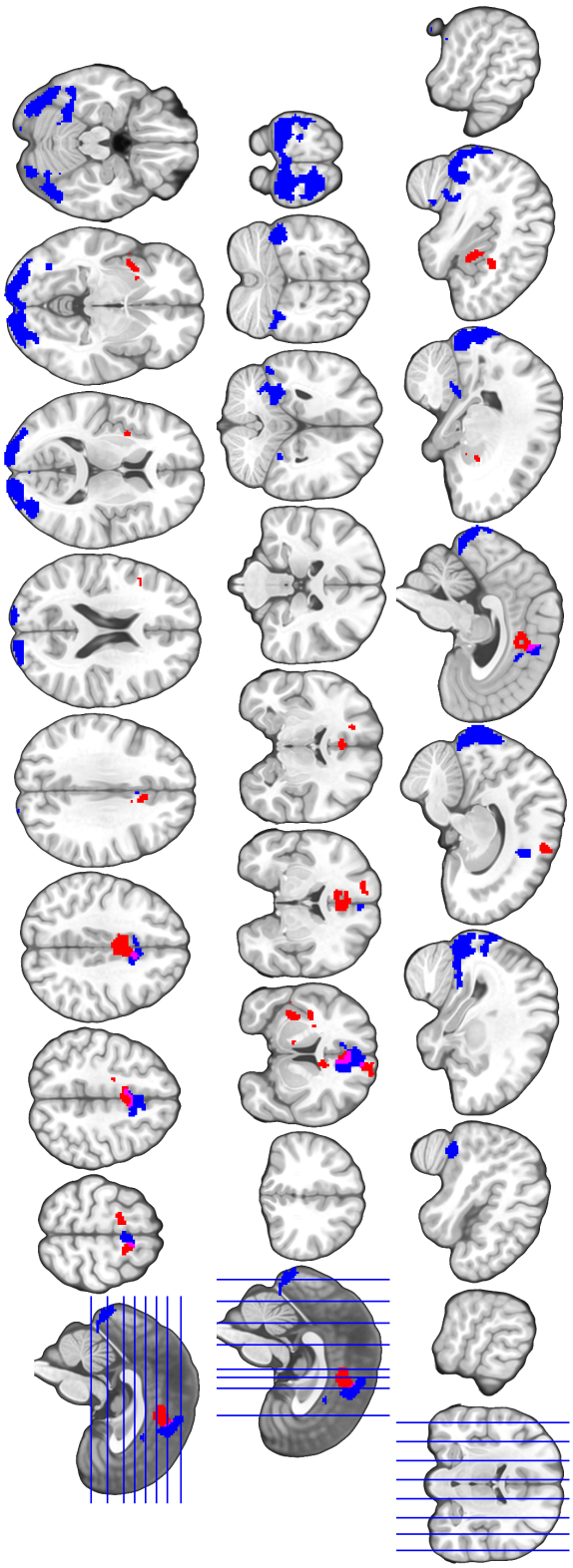

Figure 18. Comparison of the activation patterns for directly (red) and vicariously (blue) experienced pain (overlapping areas are shown in magenta). FDR-corrected ($p < 0.05$) statistically significant clusters (single-voxel $p < 0.01$) are shown for sensory pain, while FDR-corrected (single-voxel $p < 0.01$) are shown for vicarious pain.